



Relation between urban biophysical composition and dynamics of land surface temperature in the Kolkata metropolitan area: a GIS and statistical based analysis for sustainable planning

Subrata Ghosh¹ · Nilanjana Das Chatterjee¹ · Santanu Dinda¹

Received: 12 September 2018 / Accepted: 17 October 2018 / Published online: 31 October 2018
© Springer Nature Switzerland AG 2018

Abstract

The major environmental impacts of urbanization have changed urban biophysical components which ultimately promoted land surface temperature (LST) as well as urban heat island (UHI). This study explores the upshot of land use land cover (LULC) and resultant effect on biophysical components to understand the heat island mechanism in the Kolkata Metropolitan Area (KMA) for four selected time period of 1991, 2001, 2011 and 2017. Six satellite-derived biophysical components were selected for the present analysis: NDBI, NDVI, NDWI, MNDWI, NDBaI and SAVI. Selected bands of Landsat-5 TM and OLI-8 were used for this purpose. The result shows that the built-up area has been increased from 322.68 km² in 1991 to 982.86 km² in 2017 and accordingly, LST also rises from 18.47 °C mean LST of 1991 to 23.30 °C mean LST of 2017. The correlation coefficient among the biophysical parameters and LST shows that the highest continuous increasing positive relationship between NDBI and LST ($R=0.71$). Moreover, multiple linear regression model (MLR) is adapted to the prediction on LST with the variation of biophysical parameters. Finally, we produced hot spot maps using Getis-Ord-Gi* statistics for the selected year to highlights the hot spot and cold spot area in KMA. The methodology presented in this paper can be broadly applied for the planning purposes because LST monitoring is an important parameter of sustainable urban planning.

Keywords Land uses land cover change · Biophysical indices · LST · Multiple linear regression (MLR) · Hotspot-coldspot areas · Kolkata Metropolitan area

Introduction

Urbanization is the process characterized by urban land expansion and demographic changes as well as a drastic metamorphosis of land use pattern that effect on the physical boundaries of the cities (Grimm et al. 2008; Sun and Zhao 2018). Unrestrained urbanization has resulted in intensive changes in the natural landscape (Haas and Ban 2014), urban ecosystem (Zhang et al. 2017), biodiversity (Li et al. 2016a,

b), urban microclimate (Weng et al. 2008; Sannigrahi et al. 2017), and energy flow (Decker et al. 2000) in various spatio-temporal scale (Sun and Zhao 2018). According to the report of UN World Urbanization Prospects (United Nation 2014), about 54% of the world total population were residing in the urban area in 2014 and it was projected to reach up to 66% in 2050. The cities of India are no exemption of this. The urban population of India is 31.16% (Census of India 2011) and it is estimated that it will reach 66% in 2050 (United Nation 2014). Apart from this, as per Census of India 2011, the growth of urban population and urban land expansion of the large mega-cities are at an unpretending pace than the medium of small cities (Census of India 2011). According to Chen et al. (2014) the process of urbanization is the combined result of economic development, continuous migration and various socio-environmental facilities in urban areas. However, the impromptu urbanization is the focal concern of the planners because, it has several implications and impacts (Sharma et al. 2013). At the present context, urban land transformation and its impact on the urban

✉ Subrata Ghosh
subratageovu@gmail.com
Nilanjana Das Chatterjee
nilanjana_vu@mail.vidyasagar.ac.in
Santanu Dinda
santanudinda2012@gmail.com

¹ Department of Geography and Environment Management, Vidyasagar University, Midnapore, West Bengal 721102, India

landscape and urban system are the most studied phenomenon (Jiang and Tian 2010; Ng et al. 2011; Kuang 2012; Scolozzi and Geneletti 2012; Liu et al. 2016). Comprehensively studies have been done worldwide to quantify of environmental alteration due to rapid urbanization (Kates et al. 2001; Ren et al. 2003; Sharma et al. 2013; Hull et al. 2015).

The continuous and rapid urbanization can alter the numbers of physical and biological characteristics of urban landscape, including vegetation cover (Li and Liu 2017; Shifaw et al. 2018), water bodies (Yang et al. 2008; Popa et al. 2012; Sun et al. 2016; Ghosh et al. 2018), soil properties (Voogt and Oke 2003) and change of microclimate (Zhou et al. 2004; Chen et al. 2006; Li et al. 2009; Pal and Ziaul 2017) due to the expansion of impervious surface i.e. built-up area (Sharma et al. 2015; Li et al. 2016a, b; Lu et al. 2017). It is indispensable to understand the impact of urbanization on the urban environment because, the sustainable urban growth can be achieved through the proper understanding of the coupling relationship between urbanization and its environmental impact (Li and Ma 2014). In this perspective, the aim of this present study is to quantify and analyze the spatio-temporal patterns of urbanization and urban biophysical components in the city Kolkata. Generally, biophysical components are defined as a set of indicators that are able to track the human impact on a given environment (Dietz et al. 2007; Sannigrahi et al. 2017). Oke (1987) stated that the increase of impervious surface due to rapid urbanization could alter the urban biophysical components that can significantly affect Earth-Atmospheric energy process at micro scale. The mean average temperature at the local level is gradually increasing due to unprecedented change of landuse land cover (LULC) (Hoffmann et al. 2012).

Unpredicted and uncontrolled urban growth with increases of impervious area and haphazard development are the main features of Indian urbanization which causes significant decreases of agriculture land, vegetation covers,

wetland and other natural water bodies and increased pollution, slum development and various social economic problems (Sudhira et al. 2004; Rahman et al. 2011; Punia and Singh 2012). Therefore, the modern remote sensing techniques are considered as an invaluable tool for quantification and monitoring of urban land cover type with a higher level of accuracy (Bhatta 2009; Khan et al. 2017). The detailed and enhanced information can be obtained from remote sensing data, with automatic and semi-automatic techniques and this information, i.e. images can be offered from the past. Consequently, the dynamic of the urban landscape can be easily monitored (Mushore et al. 2017; Santos et al. 2017). Landsat satellite imageries (such as MSS, TM, ETM+) are extensively used as the input database for various researches to extract the urban built-up area as well as estimation of other various biophysical elements (Yeh and Li 2001; Chen et al. 2006; Bhatta 2009; Sharma et al. 2013; Bhatti and Tripathi 2014; Sun and Zhao 2018). Researchers employ various remote sensing based indices to monitor urban expansion such as Normalized Difference Built-up Index (NDBI), Normalized Difference Vegetation Index (NDVI), Normalized Difference Water Index (NDWI), Normalized Difference Bareness Index (NDBal), Modified Normalized Difference Water Index (MNDWI) etc. and their impacts (Chen et al. 2006; Sharma et al. 2013; Li and Liu 2017). Table 1 highlighted the various indices and their application in urban research along with references.

The Land surface temperature (LST) is considered as one of the important biophysical parameters for the analysis of urban health (Xiao and Weng 2007). The increase of impervious surface, i.e. built-up area due to modification and expansion of LULC in the urban area results in higher surface temperature (Qin et al. 2001; Amiri et al. 2009; Li et al. 2009; Zhou et al. 2011; Sharma et al. 2015; Wang et al. 2018). Kalnay and Cai (2003) considered that LST is one of the important indicators for monitoring urban ecological

Table 1 Different urban biophysical parameters and their applications in urban study

Indices	Application	References
NDVI	Study of vegetation cover and dynamics, productivity, phenology biomass estimation, fractal vegetation cover, urbanisation impact, analysis of surface temperature	Zhou et al. (2004), Jong et al. (2011), Liu et al. (2018), Ranagalage et al. (2018c)
NDBI	Built up area extraction, urban sprawl monitoring and study of urban heat island effect (UHI)	Zha et al. (2003), Zhang et al. (2009), Sharma et al. (2015), Sharma et al. (2015)
NDWI	Urban wetland, used for vegetation feature extraction and moisture	Maki et al. (2004), Liu et al. (2018)
NDBal	Extraction of bare land in urban area	Chen et al. (2006), Sharma et al. (2015)
SAVI ^a	Use for exclusion of soil background interference	Huete (1988)
MNDWI ^a	Enhance technique used to significantly demarcate between water bodies and others land use types	Xu (2006)

^aThese two parameters are introduced in this study as urban biophysical components and their role on controlling of land surface temperature (LST)

performance. Weng et al. (2008) stated that LST is closely associated with urban biophysical attributes such as NDVI, NDBI, NDWI, and MNDWI. Usually, LST in the urban area is higher than other non-urban area and it is known as Urban Heat Island (UHI) effect (Chen et al. 2006). The UHI is related to the intensity of the built-up area (Trlica et al. 2017). Moreover, several studies have been carried out analyzing the relation between greenness (NDVI), impervious land (NDBI) and land use and land cover changes (Chen et al. 2006; Weng et al. 2004; Xiao and Weng 2007; Zhou et al. 2011) with LST (Sandholt et al. 2002; Weng et al. 2006; Reynolds et al. 2008; Julien and Sobrino 2009; Estoque and Murayama 2017). Moreover, it is immensely important to assess the relationship among the various biophysical components with the variation of LULC. However, in this background, the present study is trying to evaluate and analyze the spatio-temporal patterns of LULC, dynamics of biophysical composition and LST and also assess the urban footprint using mixed method of remote sensing technique and statistical calculation. Moreover, researchers attempted hot spot analysis, which is also useful to assess the high concentration of the LST visually (Adeyeri et al. 2017; Tran et al. 2017).

So, there are extensive evidences of remote sensing based research on the urban biophysical composition and urban heat island phenomena (UHI) (Chen et al. 2006; Amriti et al. 2009; Sharma et al. 2013; Sannigrahi et al. 2017). Thus the study highlights the spatio-temporal dynamics of urban land use and its associated bio-physical parameters such as vegetation cover, urban water bodies, soil moisture, built-up area as well as a change of land surface temperature (LST). The two explicit objectives of this research are (a) to assess the change of urban biophysical components with the change of land use, and (b) to find out the relationship between Land Surface Temperature (LST) and urban biophysical components and their spatio-temporal patterns. Therefore, the present study may be significant of the for the sustainable urban management.

Study area

Kolkata Urban Agglomeration (KUA) known as Kolkata Metropolitan Area (KMA) is the 3rd largest Urban Agglomeration (AU) in India (Census of India 2011), spreading over 1851 Km² area situated on 22°00'19" North latitude to 23°00'01" North latitude and 88°00'04" East latitude to 88°00'33" East longitudes (Fig. 1). It has developed as a linear and contiguous urban concentration in the North–South direction along the bank of the Hoogly River in both Eastern and Western part. This urban agglomeration consists of 3 Municipal Corporation viz. Kolkata Municipal Corporation (KMC), Howrah Municipal Corporation (HMC)

and Chandannagar Municipal Corporation (CMC), and 38 municipalities which are contiguous with these 3 Municipal Corporations along with 77 Census towns i.e., non-municipal town and 16 outgrowths (UGs). Apart from this, the entire urban areas are surrounded by 445 rural villages consists of the settlement, agricultural land, and green belt. The tropical wet and dry climate is mainly dominated over the area with 1650 mm monthly temperature ranging from 18 to 35 °C. The population of this agglomeration is 14.72 Million and the average population density is 7950 persons/Km² (Census of India 2011). The projected population of Kolkata urban agglomeration for 2021 will be 21.10 Million with 1.8% annual growth rate (Census of India 2011). The high population density, compact urban growth and widespread transit network with low infrastructure only (6%) are the major spatial outlook of this agglomeration (Census of India 2011). As a progressive metropolitan, KMA is habitually faced problems like air pollution, poverty, excessive migration, increasing slum population, traffic congestion and various social economic problems (Bhatta 2009) due to rapid and unplanned urban growth (Dasgupta et al. 2013). Particularly surrounded rural areas are becoming more vulnerable in terms of loss of vegetation, natural water bodies, soil and water pollution (Ramachandra et al. 2014; Mukherjee 2015; Mithun et al. 2016).

Materials and methods

Database

Landsat images of 1991, 2001, 2011 and 2017 are used for this study. Landsat Thematic Mapper (TM) images of 1991, 2001 and 2011 and Operational Land Imager-8 (OLI-8) images for 2017 are used for measurement of urban biophysical parameters. The Thermal Infrared Sensor (TIRS) was also used for retrieval of the LST. The multi-temporal images were collected from the USA Geological Survey (<http://earthexplorer.usgs.gov/>). The collected images were pre-georeferenced to the UTM-Zone 45 North projection with WGS-84 datum (other information about collecting images are given in Table 2).

Image pre-processing

The collected images were pre-processed using ERDAS Imagine 2014 software. Spectral enhancement was done by computing band-ratoning combination with the help of vegetation indices to illustrate the relationship between various biophysical parameters like built-up intensity (NDBI), greenness (NDVI), wetness (NDWI) water bodies (MNDWI) etc. with the thermal behaviour (LST) of an urban area. No further atmospheric correction was done as the cloud-free

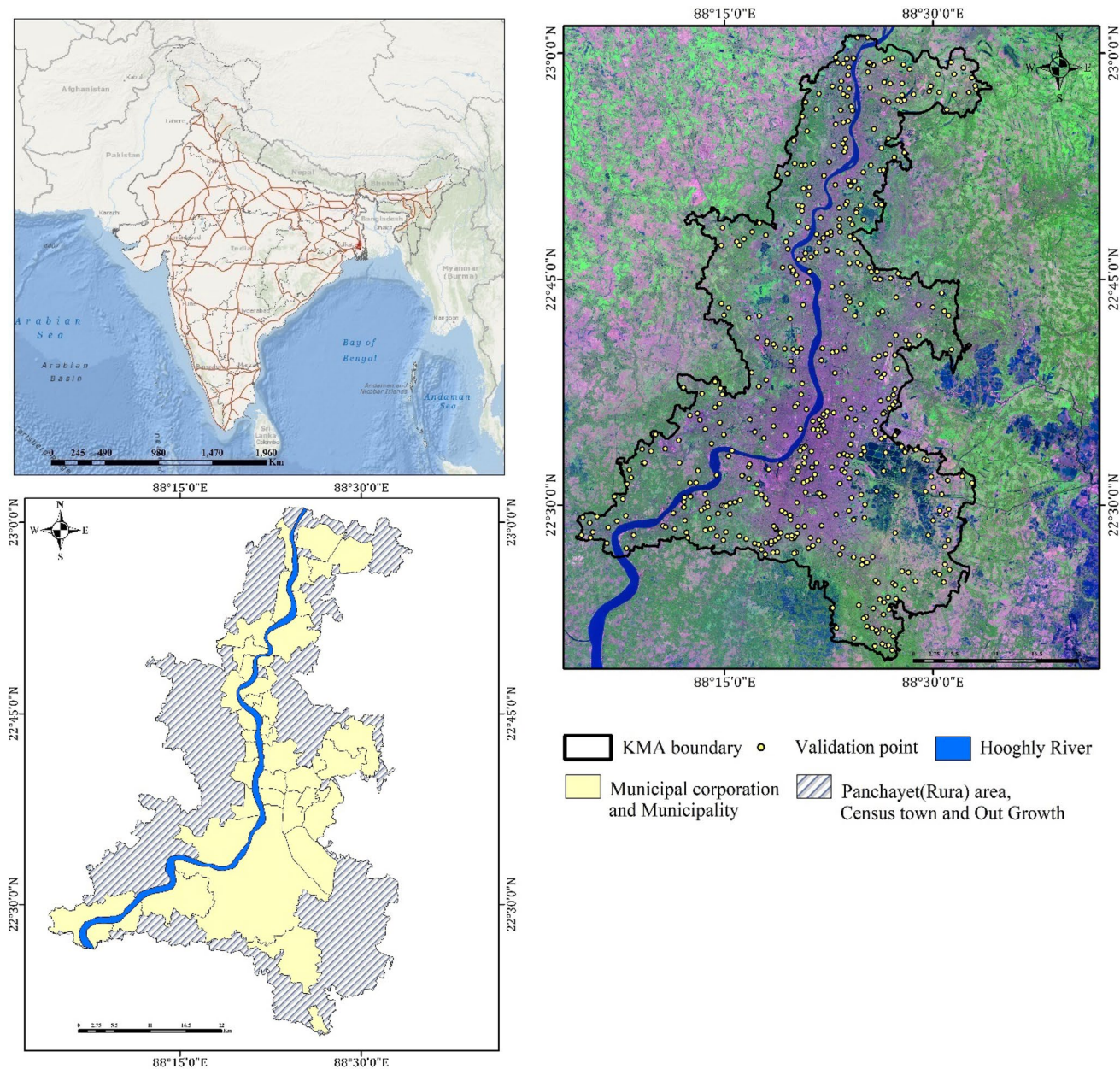


Fig. 1 Location of the study area along with different administrative boundaries and validation points

Table 2 Selected satellite data used for this analysis

Year, date and time	Satellite	Path and row	Resolution	Referencing system
1991, January 21	Landsat-5 TM	138/44 and 138/45	B, G, R, NIR, SWIR 1 and 2–30 m TIR—120 m	UTM and WGS84
2001, January 12	Landsat-5 TM	138/44 and 138/45	B, G, R, NIR, SWIR 1 and 2–30 m TIR—120 m	UTM and WGS84
2011, January 20	Landsat-5 TM	138/44 and 138/45	B, G, R, NIR, SWIR 1 and 2–30 m TIR—120 m	UTM and WGS84
2017, January 08	Landsat-8 OLI and TIRS	138/44	B, G, R, NIR, SWIR 1 and 2–30 m TIRS 1 and 2–100 m	UTM and WGS84

images were selected for analysis (Deng and Wu 2013; Bhatti and Tripathi 2014; Khan et al. 2017). The boundary of the study was clipped initially to reduce null pixels at the processing stage and the careful observation was taken during band combination from false color composition (FCC) (Zha et al. 2003). Landsat TM band 4 and 5 are most appropriate and functional to extract built-up area from other areas (Zha et al. 2003; Bhatti and Tripathi 2014; Khan et al. 2017). But OLI band is differing from TM bands, therefore, the spectral signatures of the built-up area should be checked (Bhatti and Tripathi 2014). At the same time, the other associated signatures, i.e. vegetation, built-up area, water bodies, wetness etc. should be examined for various multi-temporal images (Khan et al. 2017). Red band (Band-3, wavelength 0.63–0.69 μm) and Near-Infrared (NIR) band (Band-4, wavelength 0.76–0.90 μm) were used to identify vegetation cover in an area (Maxwell and Sylvester 2012). The built-up area was estimated by Zhang et al. (2009) using Near Infrared band (NIR) (Band-4, wavelength 0.76–0.90 μm) and Shortwave middle-infrared (SMIR) (Band-5, Wavelength 1.55–1.75 μm). But we confirmed the Digital Numbers (DN) of various land types, using 30 samples of DN values both for TM and OLI-8 bands, and plotted in Fig. 2 and it is shown that higher spectral reflectance of vegetation in both TM 4 and OLI 5 band. In this way, a positive value will be given by subtracting band 3 and 4 for TM and subtraction band 4 and 5 for OLI-8 which notably indicates the vegetation (Zha et al. 2003).

To produce thermal maps, noise reduction is required, especially for thermal infrared band (TIR) (Chen et al. 2006). The noise can be distressing through retrieval of LST and thus we adopt a self-adaptive filter method for reduction of non-periodic noise and fast fourier transform method (FTM) for removal of periodic noise. These tasks were performed by ERDAS Imagine 2014 software. The DN values of thermal bands of Landsat OLI-8 (TIRS, band 10 and 11) were converted Top of Atmosphere (ToA) reflectance and at-satellite brightness temperature in °C was determined

(USGS 2015). All the images were geometrically corrected and rectified using 450 ground control points (GCPs) collected through GPS and Google Earth (Fig. 1). All the GCPs were validated by Root Means Square Error (RMSE) and the range of RMSE is 0.30 to 0.81 pixels which are accepted for further processing (Askne et al. 2003).

Method of land uses land cover (LULC) classification

The Landsat satellite data were used to LULC classification. There have several of methods for the classification of urban LULC such as object-based classification (Drăguț and Blaschke 2006), algorithm-based classification (Mather 2004), artificial neural network (ANN) and support vector machine (Mitra et al. 2004; Van der Linden et al. 2007) etc. But supervised classification is the most useful methods for extraction of LULC map particularly in the urban area (Sahana et al. 2018). The maximum likelihood (ML) classification algorithm was adopted for supervised LULC classification as the ML algorithm is most useful and well known parametric classifiers (Otukey and Blaschke 2010). The ML algorithm is based on Bayes’ theorem for computing the most likely class (ω_j) from a set of N classes to any spectral band i.e. feature vector (x) which have a highest posterior probability, $\text{Pr}(\omega_j|x)$. Therefore, all posterior probability is calculated i.e. $\text{Pr}(\omega_j|x)$, $j \in [1]$ and highest value are selected with likely class, ω_j . The calculation of $\text{Pr}(\omega_j|x)$ is:

$$\text{Pr}(\omega_j|x) = \frac{\text{Pr}(\omega_j|x) \times \text{Pr}(\omega_j)}{\text{Pr}(x)} \tag{1}$$

Posterior probability with feature vectors (x) should be classified with most likely class (ω_j). The major advantage of this classifier is that it considered variance–covariance values within the class distribution and therefore it is well performed than other parametric classifiers (Erbek et al. 2004; ERDAS 2009). EARDAS Imagine 2014 is used to perform supervised classification. Therefore, classification

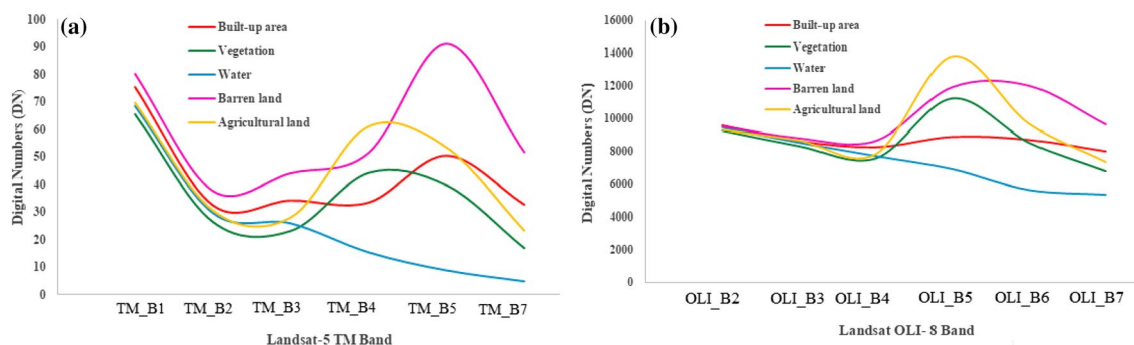


Fig. 2 Comparison of spectral signatures of built-up land, vegetation cover, water bodies, barren land and agricultural land between **a** optical bands of 1–5 and 7 of Landsat TM and **b** optical band of 2–6 and 7 of OLI-8

scheme has been developed in two stages: first, LULC types have been determined (detailed LULC classification scheme are shown in Table 3) and, then, accuracy assessment has been done through ground truth. LULC change has been calculated using a change matrix technique using ArcGIS

Accuracy assessment

Accuracy assessment is done for LULC classes and LULC change of the study area. It indicates the degree of difference between classified images and reference data. Thus, to determine the quality of information extracted from the data, classification accuracy of 1991, 2001, 2011 and 2017 images were analyzed. We use some of the accuracy statistics, namely, the overall accuracy (OA), user’s accuracy (UA), producer’s accuracy (PA) and Kappa coefficient as accuracy statistics were derived from the error matrix to assess the classification accuracies (Congalton and Green 2009)

$$OA = \frac{\text{Number of true positive} + \text{Number of true negative}}{\text{Pixels in the ground truth}} \times 100\% \tag{2}$$

UA is measuring the commission error and represent the probability of classified pixel represent the category truly on the ground when PA represents the how the classification was fit (Zhou et al. 1998). The PA and UA are derived as:

$$UA = \frac{\text{Row elements}_{diagonal}}{\text{Row}_{total}} \tag{3}$$

$$PA = \frac{\text{Column elements}_{diagonal}}{\text{Column}_{total}} \tag{4}$$

Kappa coefficient is used for measures of inter-observer agreement for characterized items and widely used for LULC accuracy assessment (Foody 1992). Kappa coefficient (K) is calculated as:

$$K = \frac{n \sum_{k=1}^q n_{kk} - \sum_{k=1}^q n_{k+n+k}}{n^2 - \sum_{k=1}^n n_{k+n+k}} \tag{5}$$

where n is the total no of pixels the references data, n_{kk} is the total no of i class, n_k is the total no of pixels for the i th class derived from the classified data, n_{+k} is the total no of pixels for the i th class derived from the reference data, q is the total no of class. The value of K with more than 0.85 is considered for excellent agreement (Monserud and Leemans 1992).

Extraction of biophysical components

Normalized difference built-up index (NDBI)

The NDBI is the important index to the extract built-up area i.e. impervious areas (Chen et al. 2006). It is efficiently used to extract built-up area from remote sensing data using the reflectance of Middle Infrared (MIR) and Near Infrared (NIR) (Zha et al. 2003). It is a common and useful technique used by the researchers for the identification of impervious surface (Zha et al. 2003; Zhang et al. 2009). The generalized

equation of NDBI is

$$NDBI = \frac{MIR - NIR}{MIR + NIR} \tag{6}$$

where MRI is the middle infrared band and (band 5 for TM and band 6 for OLI-8) and NIR is the near-infrared band (band 4 for TM and band 5 for OLI-8). The Value of NDBI range from -1 to $+1$ and values closer to 0 represents vegetation cover, the negative value represents water bodies and a positive value indicates the built-up area (Zha et al. 2003).

Normalized difference vegetation index (NDVI)

Increases of the built area can be easily comprehended by the loss of vegetation cover and NDVI is a useful technique to determine the greenness of any area (Sharma et al. 2013). It is a significant variable for the analysis of urban growth and urban micro-climatic phenomena (Chen et al. 2006).

Table 3 Various LULC classes and their descriptions

Code	LULC types	Description
1	High dense built-up area	All commercial and residential areas, transport and other infrastructure
2	Moderate dense built up area	Newly developed residential area, out growths, satellite towns, villages and transportation infrastructure
3	Vegetation and plantation	Forest, trees, shrub, planted trees, garden and parks, grassland
4	Water bodies	Rivers, wetlands, ponds, permanent open water
5	Agricultural land and	Agricultural field, crop fields and all cultivated areas
6	Barren land	Barren land, fallow land, dumping ground, open ground without grass cover

Townshend and Justice (1986) calculated a method of NDVI extraction using reflectance of NIR and red band (R). It expressed as:

$$NDVI = \frac{NIR - R}{NIR + R}, \quad (7)$$

where NIR represents band 4 for Landsat TM and band 5 for OLI-8 and R represent band 3 for TM and band 4 for OLI-8. The range of NDVI value is -1 and $+1$. The large value of NDVI indicates vegetation cover, small positive values indicate the built-up area or bare land and negative value, i.e. close to 0 indicates the water bodies (Zhang et al. 2009).

Normalized difference water index (NDWI)

NDWI is used for the assessment of liquid water present in vegetation as NDWI are directly proportional to vegetation, water content (Chen et al. 2006). The equation of NDWI was proposed by McFeeters (1996) using the reflectance of Green (G) and NIR band and it can be expressed as

$$NDWI = \frac{G - NIR}{G + NIR}, \quad (8)$$

where Green represents band 2 and NIR represent band 4 for TM and band 3 and band 5 are green and NIR band respectively for OLI-8. The value of NDWI ranges is from -1 to $+1$. Actually, NDWI is significant over NDVI because NDWI is less sensitive to the atmospheric scattering (Gábor and Jombach 2010).

Modified normalized difference water index (MNDWI)

MNDWI can be useful for estimating water bodies significantly without any built-up area and vegetation noise (Xu 2006). Here this method is used for clear identification of urban water bodies and their changing patterns. MNDWI can be expressed as

$$MNDWI = \frac{G - MIR}{G + MIR}. \quad (9)$$

Normalized difference bareness index (NDBaI)

The dynamics of NDBaI are considered as an important biophysical component for urban expansion. Chen et al. (2006) proposed the concept of NDBaI and extracted the bare land using the Eq.

$$NDBaI = \frac{SWIR 1 - TIR}{SWIR 1 + TIR}, \quad (10)$$

where SWIR 1 (shortwave infrared) represents band 5 for TM and band 6 for OLI-8 and TIR (thermal infrared) represent band 6 for TM and band 10 and 11 for OLI-8. It has

good contrast between bare land with vegetation and moist surface.

Soil adjusted vegetation index (SAVI)

SAVI as proposed by Huete (1988) to extract vegetation cover without the noise of soil background. Liu et al. (2018) used SAVI as significant indicators for land use mapping. The index of SAVI is calculated as

$$SAVI = \frac{(NIR - R)(1 + L)}{(NIR + Red + L)}, \quad (11)$$

where L is the constant value and it is basically the denominator of NDVI formula.

Extraction of LST from thermal band

The effects of the urban growth can be reflected through the change of the surface temperature. We used Landsat images after necessary correction for the determination of the LST. The step-wise procedures of LST retrieval are given below:

1. Conversion of digital number (DN) to spectral radiance ($L\lambda$)

The object having a temperature above absolute zero (K) emits energy of thermal electromagnetic appearance. Using this principle, thermal sensors were converted from sensor radiance. The spectral radiance ($L\lambda$) can be given as (Markham and Barker 1985; Avdan and Jovanovska 2016; USGS 2016)

$$L\lambda = L_{\min\lambda} + \left[\frac{(L_{\max\lambda} - L_{\min\lambda})}{(Q_{CAL\max} - Q_{CAL\min})} \times Q_{CAL} \right], \quad (12)$$

where L is the sensor-derived spectral reflectance, ($W m^{-2} sr^{-1} \mu m^{-1}$), $L_{\max\lambda}$ and $L_{\min\lambda}$ are the minimum and maximum spectral radiances for band 6 respectively. Q_{CAL} is the digital number (DN) of each pixel. $Q_{CAL\min}$ is the minimum DN value of the image, here $Q_{CAL\min} = 0$; and $Q_{CAL\max}$ is the maximum DN value of the image, here $Q_{CAL\max} = 255$.

2. Conversion of spectral radiance ($L\lambda$) to brightness temperature (T β)

It is necessary to convert spectral radiance ($L\lambda$) to reflectance (T β) for the correction of emissivity according to land use variation. According to Nichol (1994), almost a value of 0.95 is given to vegetated area and 0.92 for the non-vegetated area. The emissivity can be computed by using the formula of Artis and Carnahan (1982).

$$T\beta = \frac{K_2}{\ln\left(\frac{K_1}{L_\lambda} + 1\right)} - 273.15, \tag{13}$$

where $T\beta$ is the brightness temperature (K), L_λ represent spectral radiance of sensor ($W\ m^{-2}\ sr^{-1}\ \mu m^{-1}$) K_1 and K_2 are the calibration constant, ($K_1 = 60.776\ mW\ cm^{-2}\ sr^{-2}\ \mu m^{-1}$ and $K_2 = 1260.56\ K$ for Landsat band). An absolute zero (approx $-273.15\ ^\circ C$) should be added to revise the temperature in terms of a degree Celsius (Xu and Chen 2004).

3. Emissivity correction through NDVI method

The retrieval of the temperature value is necessary for correction of spectral emissivity (ϵ). It can be achieved through the nature of land use land cover change or by the computing of an emissivity value using NDVI of individual pixels. NDVI is important as the proportion of vegetation (P_v) should be calculated using NDVI. The NDVI is calculated by using the Eq. (6). The P_v can be calculated as

$$P_v = \left(\frac{NDVI - NDVI_{soil}}{NDVI_{veg} + NDVI_{soil}}\right)^2, \tag{14}$$

where $NDVI_{soil}$ and $NDVI_{veg}$ are the threshold values of soil pixel and the pixel of vegetation. The threshold values of $NDVI_s$ is 0.2 and $NDVI_v$ is 0.7 (Sobirno et al. 2004).

4. Land surface emissivity calculation (ϵ)

The calculation of land surface emissivity (ϵ) is important to estimate LST and it is considered as a proportionality factor of Plank’s Law i.e., blackbody radiance that predicts emitted radiance (Jiménez-Muñoz et al. 2006). The emissivity (ϵ) is calculated as

$$\epsilon\lambda = \epsilon_{veg,\lambda}P_v + \epsilon_{soil,\lambda}(1 - P_v) + C_v, \tag{15}$$

where ϵ_{veg} and ϵ_{soil} are the vegetation and soil emissivity respectively, and C is the representation of surface roughness and 0.005 is constant by the following equation

$$\epsilon\lambda = \begin{cases} \epsilon_{S\lambda} & NDVI < NDVI_{soil} \\ \epsilon_{veg,\lambda}P_v + \epsilon_{soil,\lambda}(1 - P_v) + C & NDVI \leq NDVI \leq NDVI_{veg} \\ \epsilon_{soil,\lambda} + C & NDVI > NDVI_{veg}. \end{cases} \tag{16}$$

5. Retrieval of LST

Emissivity corrected LST is the last stage of the LST retrieval and it is computed as:

$$LST = \frac{T\beta}{\left[1 + \{(\lambda \cdot T\beta / \rho) \ln \cdot \epsilon\lambda\}\right]}, \tag{17}$$

where LST means land surface temperature in $^\circ C$, $T\beta$ is the sensor brightness temperature ($^\circ C$) derived from Eq. 12, λ is the wavelength of emitted radiance in meter ($\lambda = 10.895\ \mu m$) (Markham and Barker 1985), $\epsilon\lambda$ is the emissivity determined by the Eq. (14) and,

$$\rho = h\frac{C}{\sigma} = 1.438 \times 10^{-2} mK, \tag{18}$$

where σ is the Boltzmann Constant ($1.38 \times 10^{-23}\ J\ K^{-1}$), h is the Planck’s constant ($6.626 \times 10^{-34}\ J\ K^{-1}$) and C is the velocity of light ($2.998 \times 10^8\ m\ s^{-1}$).

Statistical techniques

In order to compare the relationship between urban biophysical components and LST, we used Pearson’s correlation coefficient with R statistical programming. The 350 valid sample points were selected using systematic random sampling from the altered and unaltered areas. The extracted values of these sample points were used for correlation statistics. The LST prediction model is considered as a significant assignment for urban suitability analysis and urban sustainable planning. The regression model is considered as the most useful technique regarding this purpose (Adam and Smith 2014; Shi et al. 2018) because it is a very common, significant and suitable technique for factor based empirical down-scaling study (Crawley 2007). In this study, we used Multiple Linear Regression (MLR) model in which a dependent variable (y_i) can be explained by a linear combination with more than two independent variables (x_{in}) and it is expressed as:

$$y_i = \beta_0 + \beta_1x_{i1} + \beta_2x_{i2} + \dots + \beta_nx_{in} + \epsilon_i. \tag{19}$$

In this model, β_0 is the intercept or constant and $\beta_1, \beta_2, \dots, \beta_n$ are called regression slopes or regression coefficient estimated by ordinary least square method. ϵ_i is the error term called residuals of models. The MLR model of four selected years was validated by Durbin-Watson value and multicollinearity test.

Hotspot analysis using Getis-Ord Gi* statistics

Thermal Index is commonly used for LST to show the Urban Heat Island (UHI) effect and the impact of the change of urban biophysical composition (Mathew et al. 2017). But hot spot analysis is more useful to assess the high concentration of the LST visually (Adeyeri et al. 2017; Tran et al. 2017) Using the mean values of LST hot spot maps was produced over the study area in different periods. Hotspot analysis tool (Getis-Ord Gi*) in ArcGIS is used for this purpose. In general, the high clustered value considered as the hotspot, but it should be statistically significant (Getis and Ord 1992). Getis-Ord Gi* is calculated as:

$$G_i^* = \frac{\sum_{j=1}^n \phi_{ij} x_j - \bar{x} \sum_{j=1}^n \phi_{ij}}{\sqrt{\frac{n \sum_{j=1}^n \phi_{ij}^2 - (\sum_{j=1}^n \phi_{ij})^2}{n-1}}}, \tag{20}$$

where x_j is the attribute value for the feature j , ϕ_{ij} is the spatial weight between feature i and j , n is equal to the total number of the feature.

$$\bar{X} = \frac{\sum_{j=1}^n x_j}{n}, \tag{21}$$

and,

$$S = \sqrt{\frac{\sum_{j=1}^n x_j^2 - (\bar{X})^2}{n}}. \tag{22}$$

The output of Getis-Ord G_i^* represented by z-score and, the largest positive value of z score indicates high clustering (Wulder and Boots 1998) i.e. hotspot and the largest negative value of z-score indicate the cold spot. In this study, we categorised seven classes of hot spot and cold spot according to their significant z-value: <99% significant indicates high hot spot (z-score ≥ 2.58 , 99–95% significant indicates hot spot (z-score = 2.58 to 1.96), 95%–90% significant indicates warm spot (z-score = 1.96 to 1.65), z-value of 1.65 to – 1.65 indicates not significant, 90% significant indicates cool spot (z-score = – 1.65 to – 1.96), 90–95% significant indicates cold spot (z-score = – 1.96 to – 2.58) and >95% significant indicates highly cold spot (z-score ≤ -2.58) (Tran et al. 2017; Ranagalage et al. 2018a, b). The brief methodological highlights are shown in Fig. 3.

Results and discussion

Analysis of land uses land cover (LULC) change

Supervised land classification with maximum likelihood (ML) classification algorithm was employed to classify LULC and change pattern as it is more suitable and accurate in urban areas. First, we classify the land use types for Kolkata Metropolitan Area (KMA) into six major categories (a) highly dense built-up area, (b) moderately dense built-up area, (c) vegetation and plantation, (d) water bodies, (e) agricultural land and (f) Barren land. Wetland and river are considered underwater bodies and similarly open place and fallow lands are considered under barren land. Considering the aim of the research we have analyzed the LULC change maps for the 4 selected years, i.e. 1991, 2001, 2011 and 2017. It is seen that KMA is experiencing rapid change of its LULC dynamics in last 25 years. All the classified maps were validated using Kappa statistics, producers accuracy,

users accuracy and overall accuracy. The overall accuracy for LULC classifications are 90.22%, 92.00%, 94.22% and 96.78% for the 1991, 2001, 2011 and 2017 respectively. Similarly, Kappa coefficients for the four classified LULC maps are 0.882 (in 1991), 0.904 (in 2001), 0.930 (in 2011) and 0.951 (in 2017) respectively, which indicates that the output LULC maps can be significantly used. The producer accuracy and user’s accuracy of each LULC categories are shown in Table 4. Thus the calculated parameters and change patterns can be used for further analysis. The patterns of LULC and their area are tabulated which offers a comprehensive database for analysis in spatio-temporal dimensions (Table 5). It is seen that the total built-up area has been continuously increasing between 1991 and 2017. The built-up area has been increased from 322.68 to 982.86 Km² with a significant encroachment of open space, agricultural land and vegetation area. Thus the barren land, vegetation cover and agricultural land have significantly decreased from 1991 to 2017 are – 10.83%, – 16.08% and – 12.09% respectively. Similarly, water bodies, particularly wetland area also decreased (– 1.34%). The patterns of land use at different time periods were shown in Fig. 4.

So, the results revealed that the drastic positive change occurs in the built-up area as it is continuously increasing in different time nodes (i.e. 1991, 2001, 2011 and 2017). The growth of population and various developmental activities tend to the expansion of urban area is not only the city core, but also the periphery of KMA (Sahana et al. 2018). Consequently, vegetation cover, agricultural land, and barren land continuously decreasing.

Dynamics of bio-physical indices

The six major biophysical parameters were used for the analysis of urban dynamics and the spatio-temporal urbanization footprint. NDBI, NDVI, MNDWI, NDBaI, SAVI and NDWI are considered as the major components of the urban landscape. It is seen that the NDBI which designates the built-up area and it is gradually increasing with different time periods. The range of NDBI value of 1991 was – 0.07 to 0.64 with the mean value of – 0.042 ($SD = 0.137$). The mean value of NDBI is increasing with the rapid urbanization and the value of mean NDBI were 0.017 ($SD = 0.159$), 0.031 ($SD = 0.183$) and – 0.104 ($SD = 0.098$) for the year of 2001, 2011 and 2017 respectively. The range of NDBI value in 2017 is 0–0.53. The expansion of the built-up area has been continuously extended in Northern, South-eastern and Western direction (Fig. 5). Consequently, NDVI and SAVI are gradually decreasing in response to built-up expansion. The decreasing pattern of NDVI is evidently identified by the NDVI maps. The mean value of NDVI are 0.121 ($SD = 0.148$), 0.098 ($SD = 0.124$), 0.083 ($SD = 0.077$) and

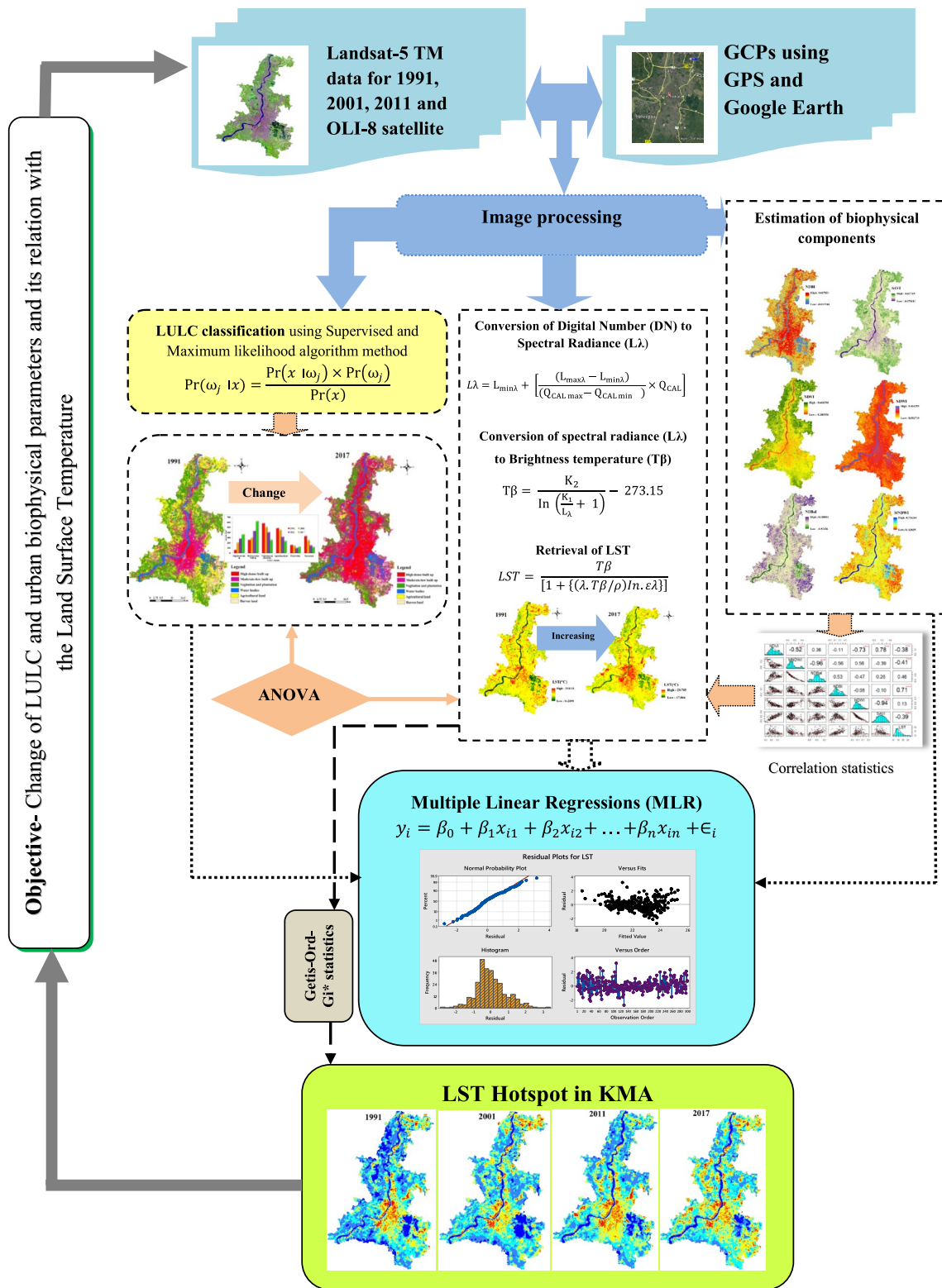


Fig. 3 Methodological work flow of this study

Table 4 Accuracy assessment table for the classified LULC maps of 1991, 2001, 2011 and 2017

Year	User’s accuracy (%)						Producer’s accuracy (%)						Overall accuracy (%)	Kappa Coefficient
	1	2	3	4	5	6	1	2	3	4	5	6		
1991	90.59	91.30	87.36	89.47	92.54	90.91	96.25	86.30	89.41	86.08	88.57	95.24	90.22	0.882
2001	91.11	92.00	92.68	88.00	95.38	93.65	96.47	90.79	91.57	90.41	87.32	95.16	92.00	0.904
2011	95.79	97.50	90.24	90.28	98.36	93.33	98.91	93.98	94.87	89.04	95.24	91.80	94.22	0.930
2017	95.10	95.29	94.81	97.06	98.25	96.72	96.04	94.19	97.33	94.29	98.25	96.72	96.78	0.951

LULC Codes: 1, high dense built-up; 2, moderate dense built-up; 3, vegetation and plantation; 4, agricultural land; 5, water bodies; 6, barren land

Table 5 Area under various LULC classes and changes of area from 1991 to 2017 in KMA

Types	1991		2001		2011		2017		Rate of change (%) from 1991 to 2017
	Area (Km ²)	% of Area	Area (Km ²)	% of Area	Area (Km ²)	% of Area	Area (Km ²)	% of Area	
High dense built-up	64.80	3.45	204.48	11.08	282.42	16.71	362.55	21.21	17.76
Moderate dense built-up	257.88	13.72	297.53	16.12	431.25	25.52	620.31	36.29	22.57
Vegetation and plantation	582.42	30.98	505.38	27.39	406.36	24.05	254.70	14.90	−16.08
Agricultural land	484.68	25.78	447.37	24.24	317.30	18.78	234.07	13.69	−T12.09
Water bodies	157.97	8.40	141.31	7.66	100.52	5.95	120.64	7.06	−1.34
Barren land	332.32	17.68	249.36	13.51	151.86	8.99	117.03	6.85	−10.83

0.075 ($SD = 0.125$) for the year 1991, 2001, 2011 and 2017 respectively. The mean value of SAVI is also representing a decreasing trend. Therefore, the vegetation cover of KMA is continuously decreasing. Here we applied SAVI as an enhanced accurate method of vegetation estimation (Shifaw et al. 2018). The mean value of SAVI are 0.152 ($SD = 0.185$), 0.142 ($SD = 0.178$), 0.129 ($SD = 0.224$) and 0.117 ($SD = 0.105$) respectively. The MNDWI, NDWI and NDBaI are also following the similar trend which indicates urban expansion in an exceeding manner with the loss of biophysical components. The mean value of MNDWI decreased from -0.126 in 1991 to -0.020 in 2017 ($SD = 0.217$). The bareness index (NDBaI) is also continuously decreasing i.e. -0.534 ($SD = 0.008$) in 1991 to -0.264 ($SD = 0.081$) in 2017 due to the encroachment of built-up area which is validated by LULC maps. However, the change of these biophysical indices demonstrated the rapid urbanizing situation in the KMA in a small time period. For the demonstration of the dynamics of various biophysical components, we carried out correlation statistics using 350 sample points (discussed in Sect. 3.7). The analysis shows that NDBI is negatively correlated with NDVI, NDWI, MNDWI and SAVI. It is seen that the correlation coefficient between NDVI and NDBI are increased from -0.02 in 1991 (which is not significant) to -0.47 in 2017 (which is significant with $p < 0.05$) that indicates the

impact of built-up expansion. SAVI, NDWI and MNDWI are following the increasing negative relationship with NDBI (Fig. 5). Hence this analysis concluded that water bodies, open land and vegetation cover are gradually transformed into built-up areas. Therefore, environmental components are highly reactive to the stimuli of urbanization.

The relationship between urban biophysical composition and LST

The rapid change of urban environment due to urbanization could be effected on the urban landscape. The land surface temperatures (LST) are gradually increasing with the increases of the urban impervious surface (UIA) i.e built-up area and the phenomena are known as Urban Heat Island effect (UHI) (Owen et al. 1998). Identifying the change of LST is one of the major objectives of this research. To assess this, we performed Pearson’s correlation statistics to show the relationship between LST and other selected biophysical components. It is evident from Fig. 5 that NDVI, MNDWI, SAVI, NDWI, and NDBaI are more dynamic over the built-up area. The LST is radically controlled by surface moisture content, vegetation cover, surface water bodies and the amount of impervious surface etc. (Guo et al. 2016). Accordingly, LST has varied in different places across the study area. The mean LST are 18.47 °C ($SD = 1.495$),

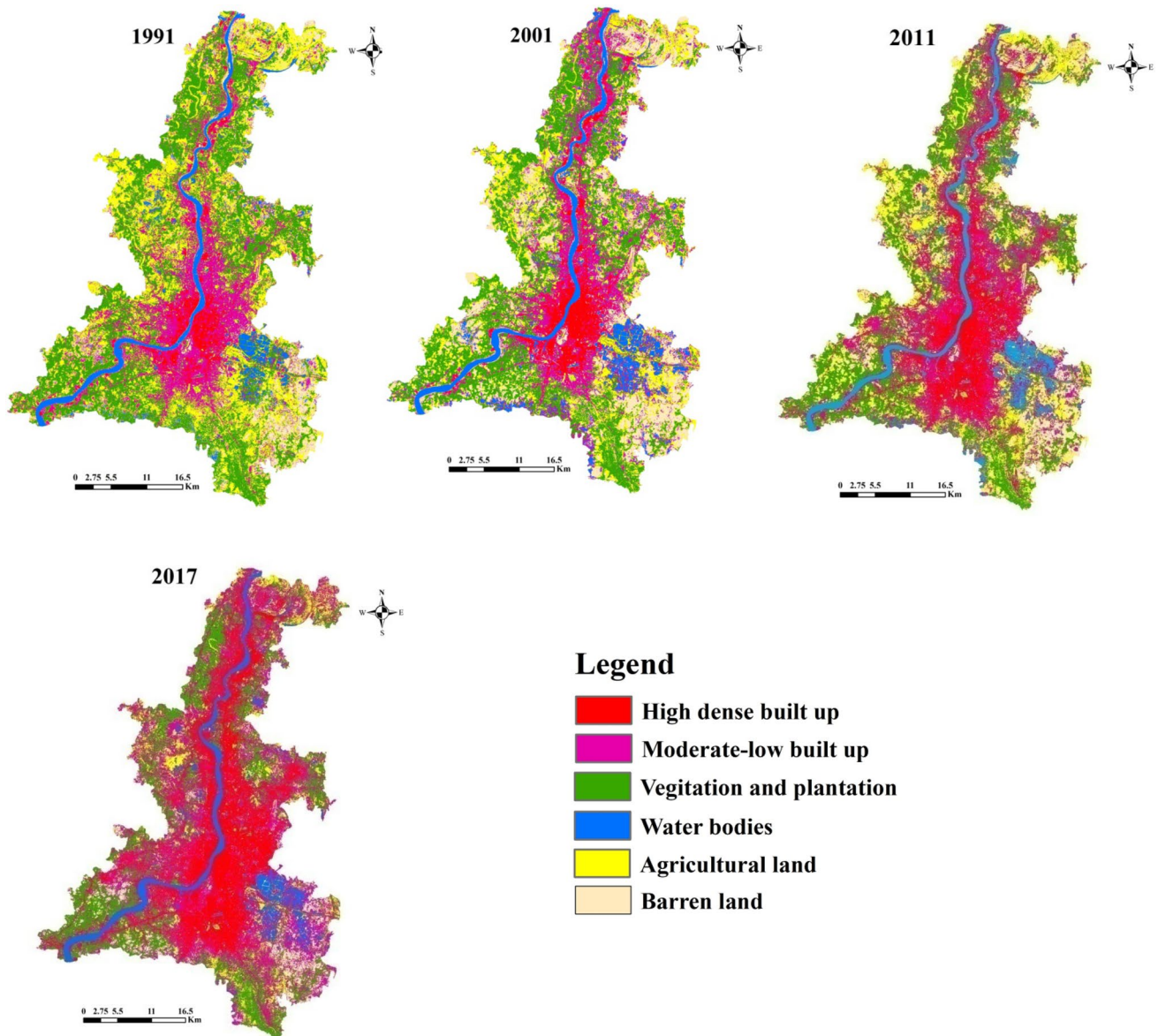


Fig. 4 Land use land cover maps of KMA showing the patterns of land use dynamics in four different time periods i.e. 1991, 2001, 2011 and 2017

18.39 °C ($SD = 1.370$), 21.04 °C ($SD = 1.719$) and 23.30 °C ($SD = 0.093$) in 1991, 2001, 2011 and 2017 respectively. Therefore, it is seen that, mean LST is gradually increasing over the last 25 years. Here it should be elucidated that, we only measured the changes of LST over different time periods and thus we considered only winter season (January) for this purpose because, the intensity of UHI effect can be clearly depicted in this season (Sharma et al. 2015). The highest value of LST is gradually increasing i.e. 25.83 °C, 26.68 °C, 28.35 °C and 29.78 °C in 1991, 2001, 2011 and 2017 respectively (Fig. 6). Among the six biophysical parameters, NDVI, SAVI, NDWI and MNDWI are negatively correlated with LST. The distribution of vegetation

cover and water bodies can reduce the surface heat of a landscape (Deng and Wu 2013; Li et al. 2016a, b; Shiflett et al. 2017). But the degree of these correlations is gradually decreased from 1991 to 2017. The correlation between NDVI and LST was (R) -0.56 and -0.51 in 1991 and 2001 respectively (Fig. 7), which are significant with p value 0.01 and also similar to the result of Yue et al. (2007), Zhu et al. (2013) and Guo et al. (2015). However, it should be illustrated that the value of the correlation (R) between NDVI and LST is gradually decreasing from -0.51 in 2001 to -0.38 in 2017 due to a considerable decrease of vegetation cover due to unremitting urban expansion. Similarly, the correlation between SAVI and LST have significantly decreased

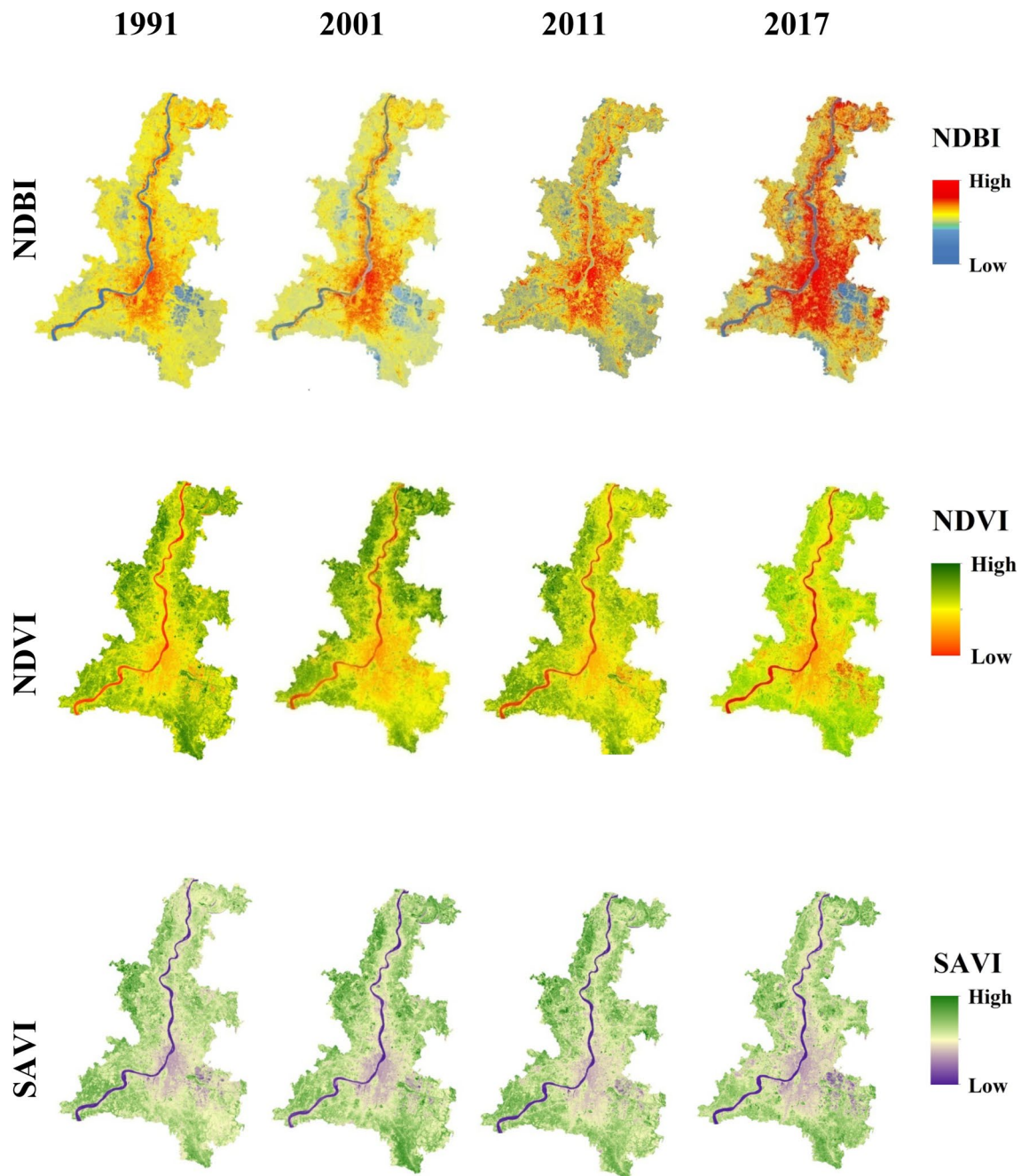


Fig. 5 Composition of urban biophysical elements and their spatio-temporal dynamics over the KMA

from 1991 to 2017. The patterns of correlation between MNDWI and LST are -0.45 , -0.44 , -0.40 and -0.41 in 1991, 2001, 2011 and 2017 respectively, which indicate a decrease of water bodies and increase LST (Fig. 7).

We introduced NDBI and NDBaI to accurately demarcate the built-up area and bare land respectively because the spectral reflectance of built-up area and bare land are too difficult to separate. However, NDBaI is positively related to LST and the value of the correlation coefficient (R) is

0.49 , 0.50 , 0.47 and 0.46 in 1991, 2001, 2011 and 2017 respectively. But the relationship between NDBI and LST are significantly positive with a range of 0.60 – 0.95 (Chen et al. 2006; Sannigrahi et al. 2017). In this study, the range between NDBI and LST are 0.53 to 0.71 ($p \leq 0.01$). The value of correlation coefficient is gradually increasing i.e. 0.53 in 1991, 0.58 in 2001, 0.67 in 2011 and 0.71 in 2017 respectively (Fig. 7). Accordingly, LST significantly varied with the variation of urban biophysical composition. The,

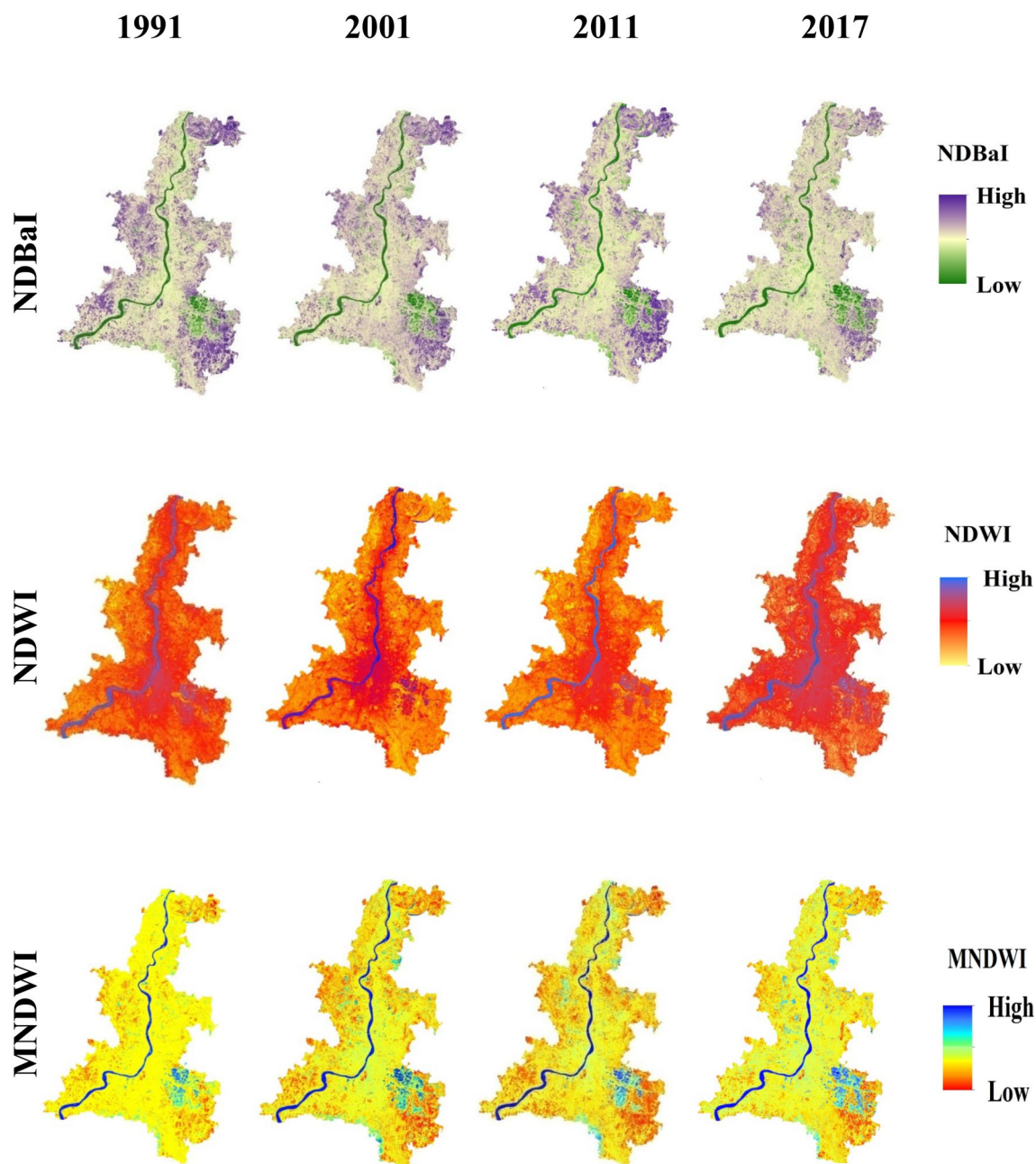


Fig. 5 (continued)

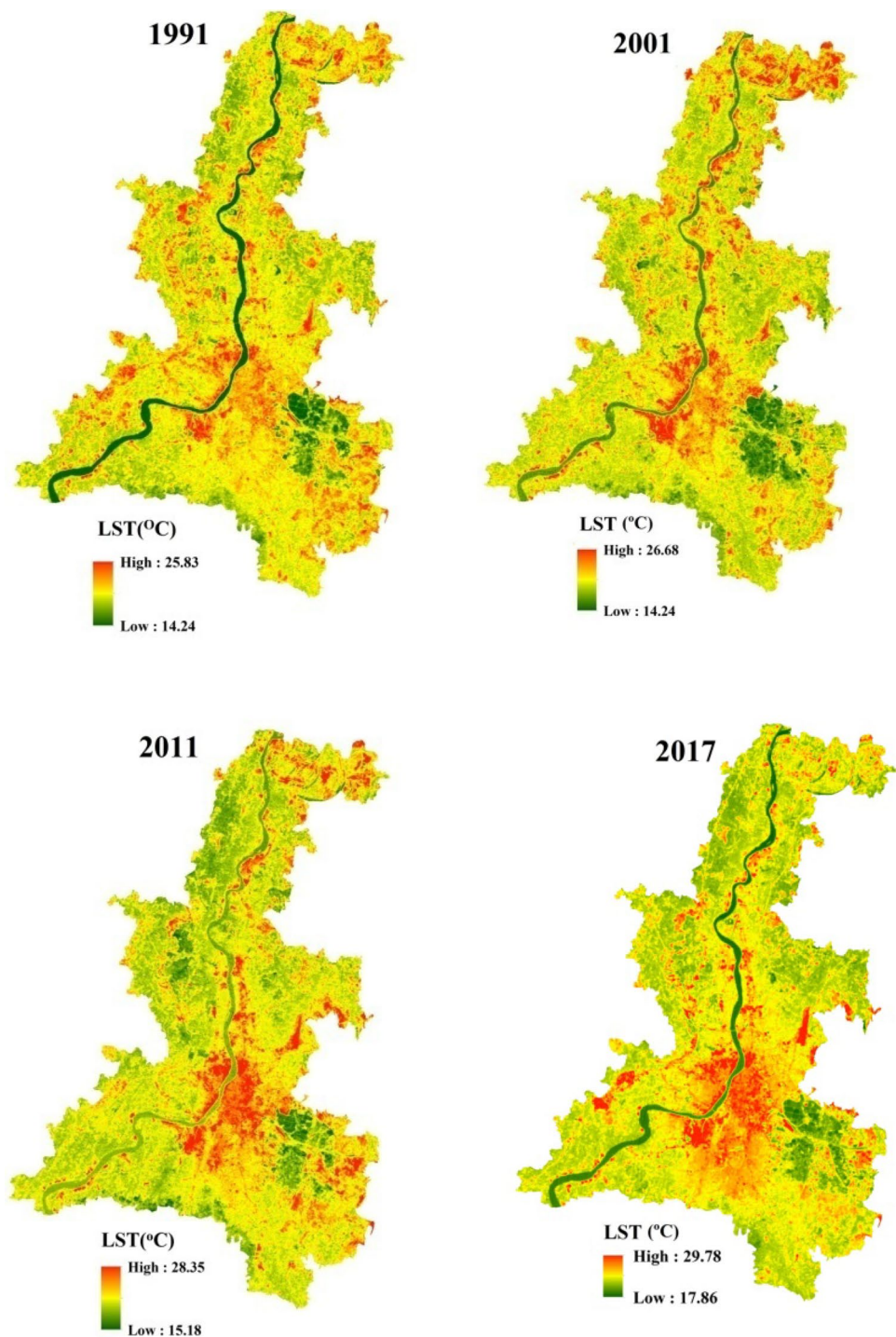
cross-sectional profiles of LST are also showing the changes of LST in different landuses over four selected periods (Fig. 8). The core area are shows higher LST than surrounding rural due to UHI effect (Ranagalage et al. 2018a, b).

Multiple linear regression (MLR) model for LST prediction

The LST is contrasted with the variation of LULC and its spatio-temporal dynamics. No doubt, urban biophysical

parameters are considered as the predictor variables of the LST. LST is positively correlated with the built-up areas and bare land and negatively correlated with water bodies and vegetation. Thus, it is significant to study all the predictors which are controlling of LST rather than single variable. The multiple linear regression (MLR) model has been used to find out the relationship between dependency and all independent variables and their role in controlling the LST (Connors et al. 2013). MLR is a significant tool that can easily predict LST and its changing pattern using

Fig. 6 LST maps of KMA in different time periods. The mean LST are 18.47 °C, 18.39 °C, 21.04 °C and 23.30 °C in 1991, 2001, 2011 and 2017 respectively shows a continuing rising trend



the selected control's variables, i.e NDBI, NDBaI, NDWI, MNDWI, NDVI, and SAVI. MLR has been done for four selected time periods to characterize the variability of LST with the changeability of biophysical composition. The Table 6 shows the results of MLR. It can be explained from the table that, the coefficient of NDBI is always an important factor in predicting LST in different years. The MLR model of the year 1991, we got the correlation coefficient,

$R=0.715$ and coefficient of determination, $R^2=0.512$, i.e. 51.20%, and the predicted $R^2=51.75\%$. Similarly, The correlation coefficient of the variables for the year 2001, $R=0.751$ and the correlation of determination, $R^2=0.564$, i.e. 56.40% and predicted $R^2=54.89\%$. So the correlation coefficient value of the MLR model with two time periods (i.e. 1991 and 2001) are not well fitted to the data. That indicated independent variables are not significantly describing

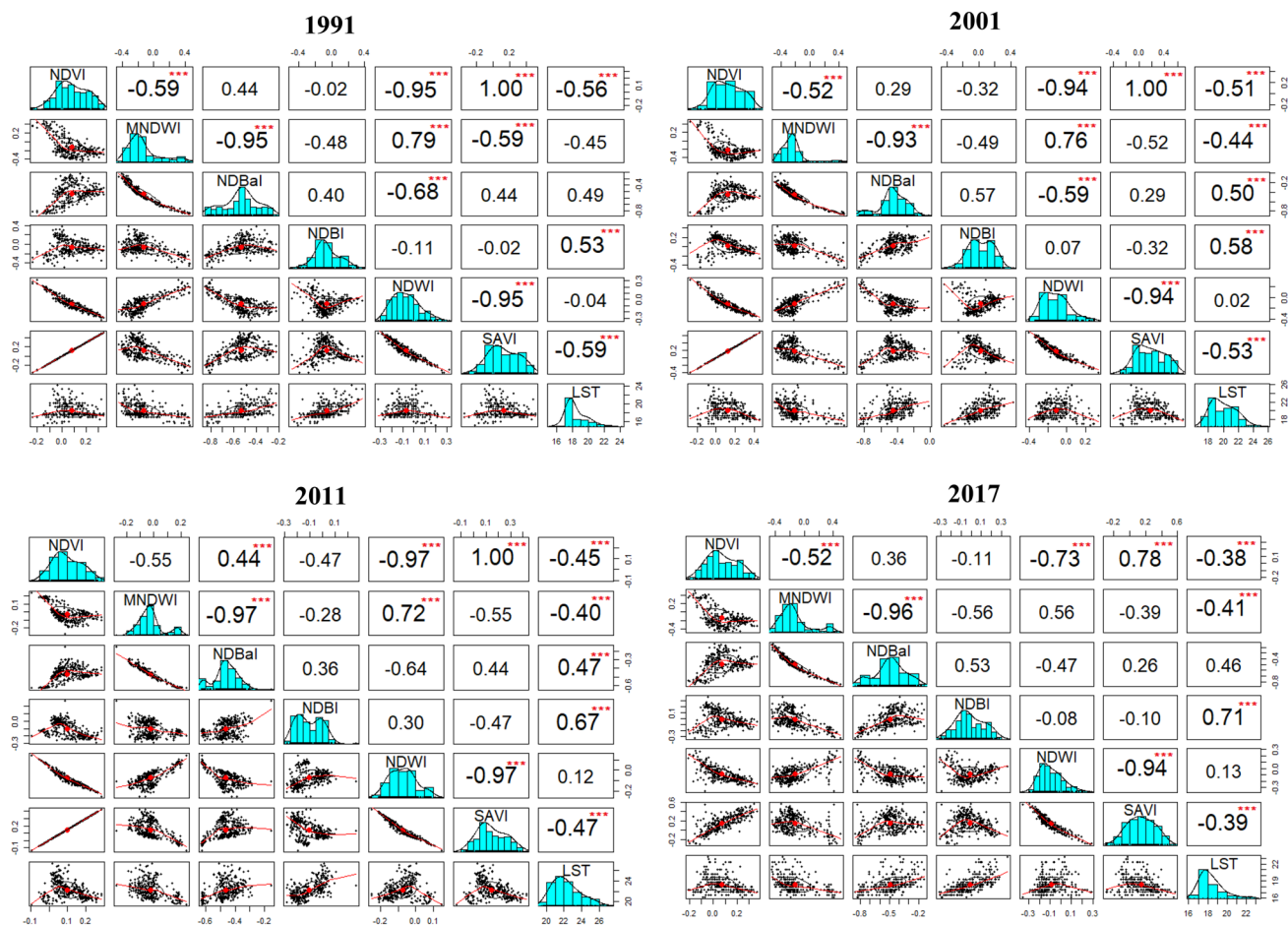


Fig. 7 Correlation coefficient graph to showing the relationship between of urban biophysical parameters and LST in different time periods (***) significance level = $p < 0.01$)

the dependent variable. Actually, the built-up areas are not significantly increasing and vegetation and water bodies remarkably existed. Therefore, the variation of LST cannot be significantly represented by the correlation coefficient values. But the results of 2011 and 2017 indicate a significant correlation coefficient among the variables ($> 60\%$). The correlation coefficient of the year is $R = 0.791$ in 2011 and coefficient of determination, $R^2 = 0.626$ i.e. 62.60% and the predicted $R^2 = 60.16\%$, which represent that controlling variables are significantly defined the patterns and distribution of LST with the p -value of < 0.001 . Similarly the R -value of the year 2017 is 0.864 and the $R^2 = 0.716$ i.e. 71.60% and the predicted $R^2 = 69.93\%$. So the coefficient value indicates a good fit for the linear model. It represents 71.60% of the variance of the dependent variables (Table 6). Consequently, it can be explained that, rapidly increasing built-up area, decreasing vegetation and water bodies are the causes for raising the LST in the study area.

Assessment of model fit

We performed numerous statistical test to validate and predict the applicability of the selected MLR model. We performed a t -test for the selected years and the value is $(t_i) > 2.0$ with $\alpha < 0.001$ significance level that signifies the importance of selected variables of the model. The Durbin-Watson ($D-W$) values are 1.743, 1.795, 1.866 and 1.876 for the year of 1991, 2001, 2011 and 2017 respectively. It shows that, as the $D-W$ values are close to 2, therefore, the residuals are independent. The linearity of each model was checked by fitting value versus residual values, observation order versus residual order and frequency histogram of residual (Fig. 9). The Centered Leverage value and the Cook's distance are in an acceptable range. Thus the regression model does not affect by Outliers. Variance inflation factors (VIF) and Tolerance value are used to measure the multicollinearity. The normal probability plots of the linear regression model indicate the residual called error a term that is normally distributed

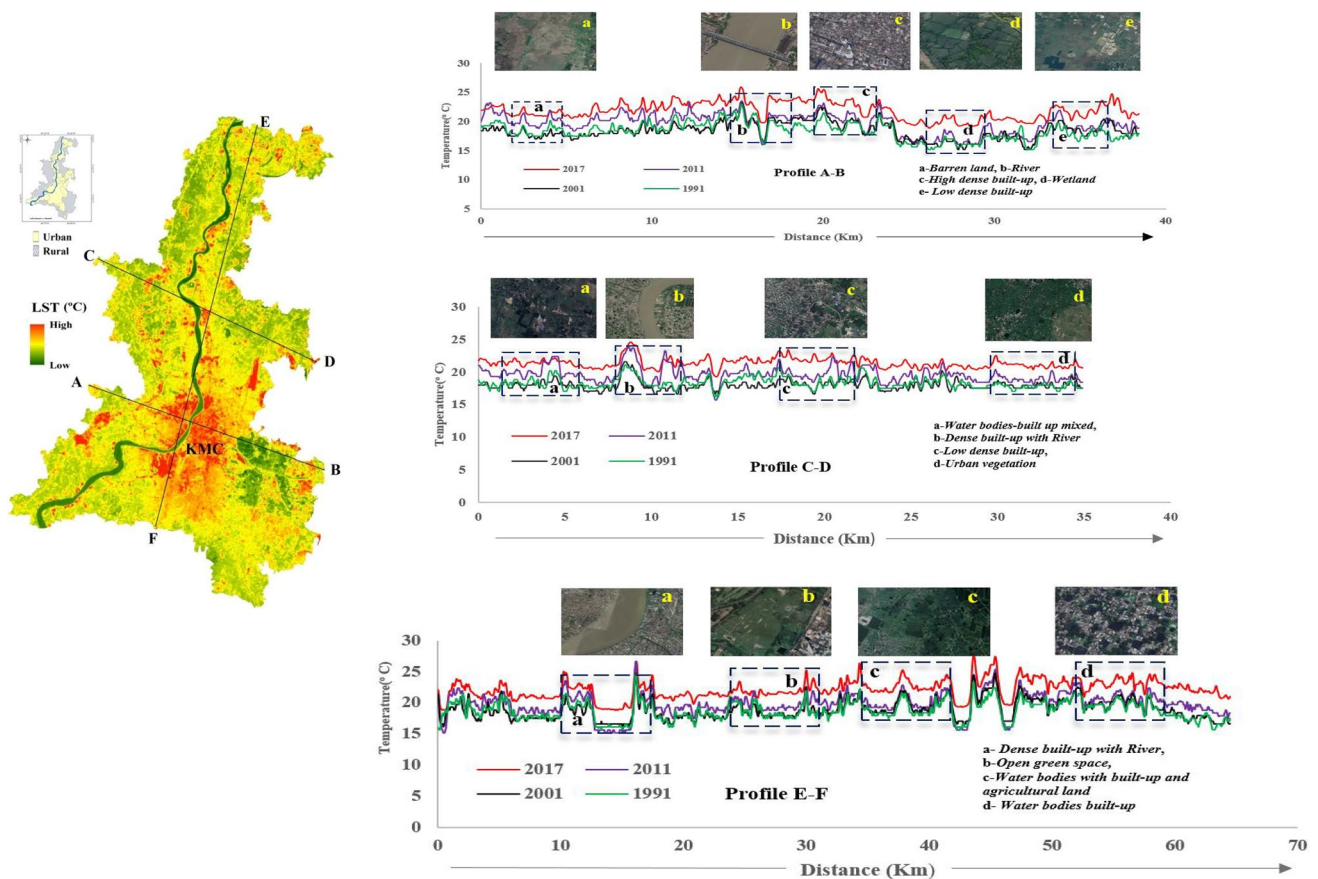


Fig. 8 LST profiles of three selected rural–urban gradients, characterized by different LULC in four selected time periods. The marking a–e indicates, various LULC and their respective LST. The comparisons of LST graph indicated continuously rising of LST

Table 6 Multiple linear regression equation showing the R^2 and predicted R^2 values of predictors variables of LST

Year	Regression equation	R	R^2	R^2 (predicted)	p-value
1991	$LST = 18.51 + 2.090 NDBI + 0.858 NDBaI - 7.157 NDWI - 3.979 MNDWI - 13.903 NDVI - 8.130 SAVI$	0.715	0.512	51.75%	<0.001
2001	$LST = 17.726 + 2.726 NDBI + 1.360 NDBaI - 1.912 NDWI - 4.143 MNDWI - 4.004 NDVI - 2.794 SAVI$	0.752	0.564	54.89%	<0.001
2011	$LST = 14.469 + 0.886 NDBI + 1.772 NDBaI - 11.570 NDWI - 3.570 MNDWI - 2.726 NDVI - 3.483 SAVI$	0.791	0.626	60.16%	<0.001
2017	$LST = 11.126 + 3.141 NDBI - 8.847 NDBaI - 25.385 NDWI - 44.00 MNDWI - 28.341 NDVI - 18.891 SAVI$	0.846	0.716	69.73%	<0.001

and follows a straight line, particularly the model for the year of 2011 and 2017 (Fig. 9). It signifies that the distribution is a good fit and the model can be accepted.

Hotspot analysis of LST in KMA

The hot spot analysis has been done to indicate the area affected by increasing LST. The hot spot maps were prepared for four selected time periods and each of the maps was significant of $p < 0.0001$. The hot spot maps show that

maximum hot spot was founded in the built-up area and the low spot was mainly dominated over the vegetation and water bodies which indicated the maximum clustering of high and low LST pixels in those areas respectively. It is clearly seen that the vegetation and water bodies have a significant role in controlling LST. Hotspot map of 1991 clearly indicates that the high values of LST are mainly concentrated over the core built-up areas and cool spot were dominated over the water bodies study area. The maps for respective years clearly visualize the change of the cold spot area

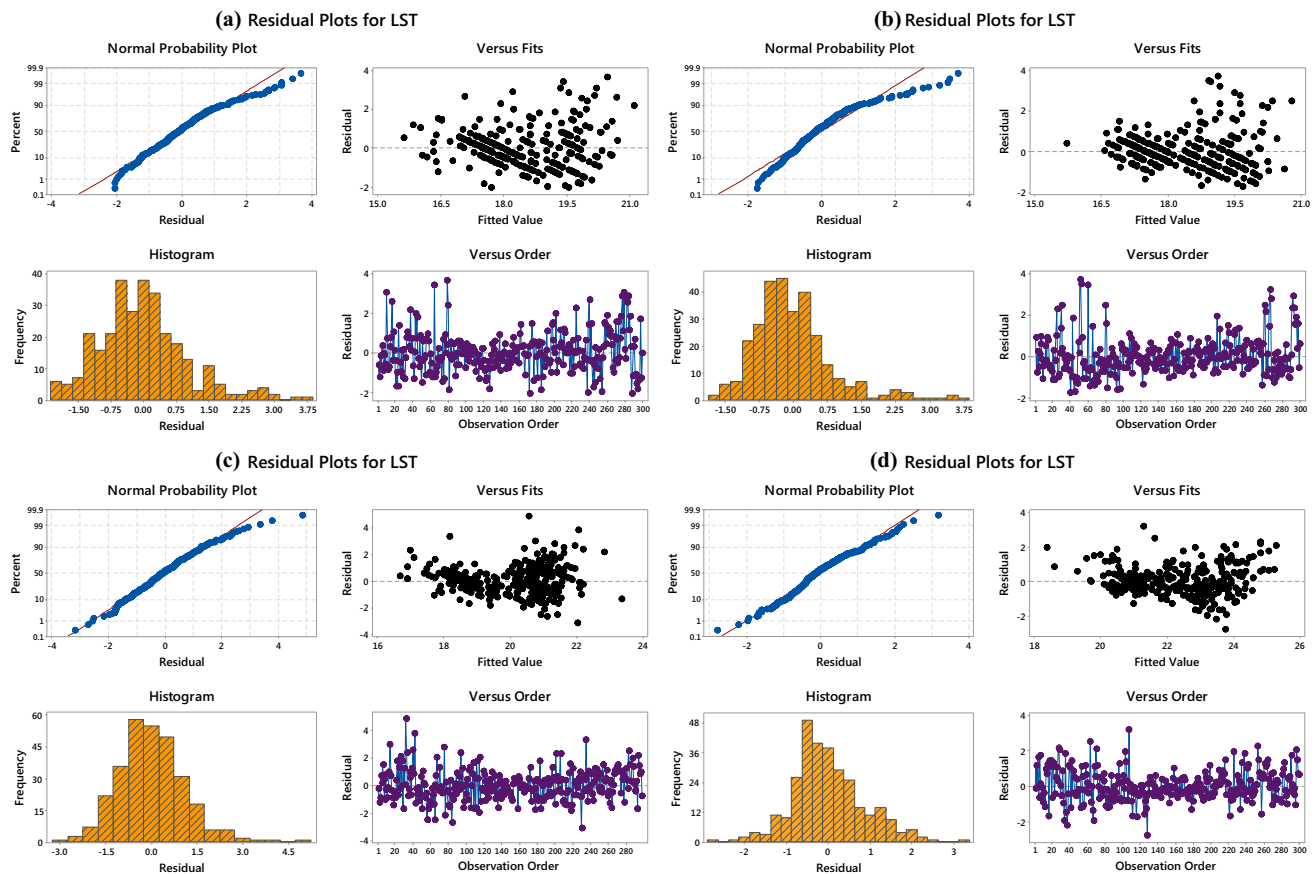


Fig. 9 Results of MLR representing normal probability plots, residuals, versus order and versus fits for four selected time periods **a** 1991, **b** 2001, **c** 2011 and **d** 2017

in hot and highly hot-spot area (Fig. 10). Accordingly, with the increasing of built-up area, the hot spot areas are also extended from the core area to peripheral areas. However, the hotspot analysis can clearly depict the existing situation of LST in KMA and its related vulnerability. Thus, hot spot maps can be helpful for assessment of LST exposure as well as ecological assessment can also be possible for sustainable urban growth.

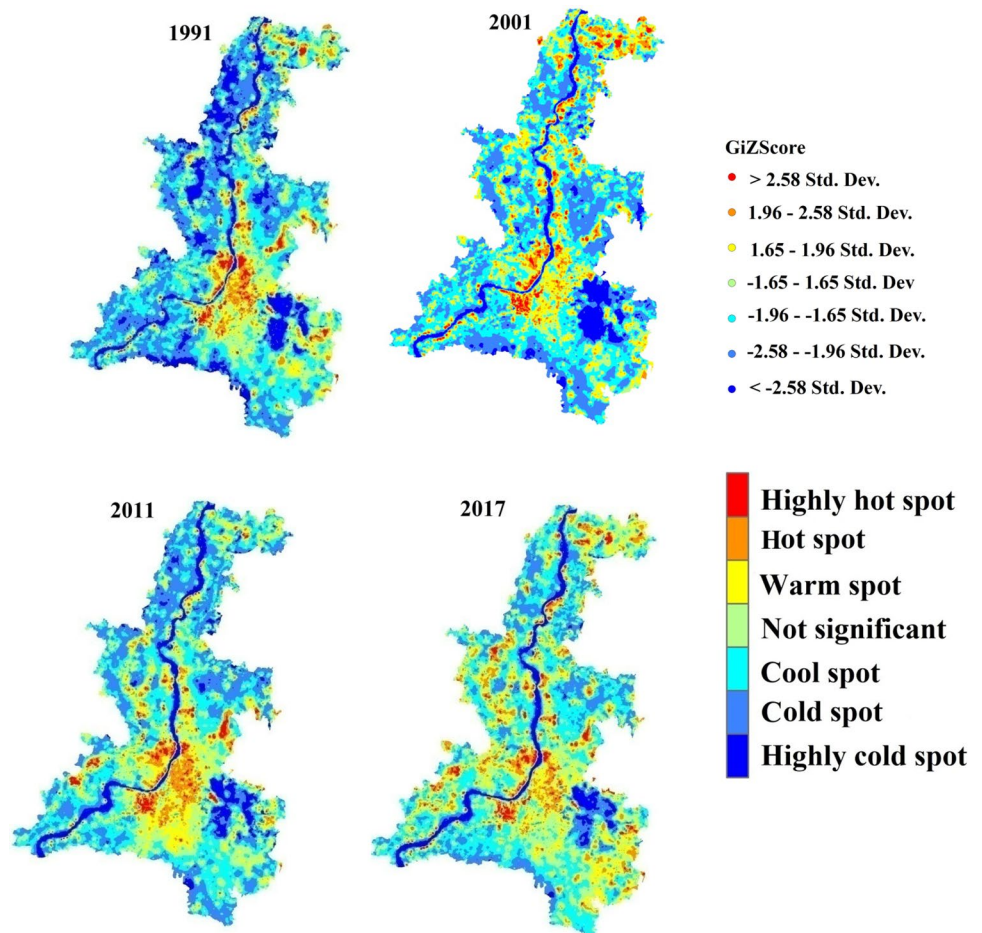
Conclusion

In this study, we have assessed the spatiotemporal pattern of land use dynamics and its response to urban biophysical compositions. Simultaneously, we have been trying to assess the relationship between urban biophysical components and the rising trend of the LST. As a megacity and 3rd largest urban agglomeration, KMA is facing a continuous influx of population and resultant continuous expansion of the built-up area. LULC maps of KMA show that KMA faces the rapid change of LULC after 2001. The built-up area of

the KMA is rapidly increasing from 322.68 Km² in 1991 to 982.86 Km² in 2017. The urban biophysical parameters significantly respond to the change of LULC. It is seen from the analysis that, vegetation cover, agricultural land and water bodies are significantly decreased. Consequently, LST of the entire study area is continuously increasing from 18.47 °C mean LST of 1991 to 23.30 °C mean LST in 2017.

This analysis is based on modern comprehensive approaches combining of geospatial and statistical methods. Remote sensing and GIS-based analysis are useful and effective for such a study. Among the existing biophysical indices, which are already used by the scholars, we have introduced two related parameters i.e. SAVI and NDBaI in this study. The methodological pathway was clear to recognize and successfully convene with the objectives. The statistical tools combining correlation statistics, MLR and Getis-Ord-Gi* statistics have been successfully investigated the targeted analysis. The result shows that among the six biophysical parameters NDBI is considered the most important controlling variables as the correlation between NDBI and LST are gradually increasing from 1991 to 2017. MLR is adopted for

Fig. 10 Hot spot and cold spot maps of KMA for four time periods showing the hot spot areas are gradually extending towards cold spot areas



prediction of LST using selected bio-physical factors. The result of the MLR of 2017 shows that LST is significantly predicted by the predictor variables ($R^2 = 71.60\%$). Thus, it is established that the change of LST is gradually increasing with the changes in biophysical components.

A continuous, suitable and conservation policy actions should be taken to minimize urbanization impacts. At the issue of policy action, KMA comes under the Kolkata Municipal Development Authority (KMDA), but the KMDA consists of several legal institutions, such as KMC, HMC, CMC, West Bengal Housing, and Infrastructure Development Corporation (WBHIDCO), various municipal offices and punched offices. The management plans should be taken by collaborating these authorities for sustainable urban growth. Moreover, some initiatives have been taken by KMDA, for example, Land Use and Development Control Plan including demarcation of development control zones, housing regulation, conservation of green space etc. (KMDA 2016). However, some management options can be summed up for sustainable development of KMA:

(a) Proper land use planning and regulation should be implemented without destroying natural biodiversity.

- (b) The conservation of open place and green space should be strictly maintained to reduce the impact of the LST.
- (c) Construction of housing and building materials should be scientifically used and well planned for reduction of surface temperature.
- (d) The proper zoning system should be done according to the adjoining ecosystem and their resilience capacity.
- (e) Moreover, a comprehensive plan should be taken and must be implemented rather than a township plan.

Acknowledgements The authors acknowledge to USGS for providing Landsat data. The authors Ghosh, S and Dinda, S are thankful to the University Grant Commission (UGC) for providing research grant.

Compliance with ethical standards

Conflict of interest The authors have declared that, there has no potential conflict of interest.

References

- Adams MP, Smith PL (2014) A systematic approach to model the influence of the type and density of vegetation cover on urban heat using remote sensing. *Landsat Urban Plan* 132:47–54. <https://doi.org/10.1016/j.landurbplan.2014.08.008>
- Adeyeri OE, Akinsanola AA, Ishola KA (2017) Investigating surface urban heat island characteristics over Abuja, Nigeria: relationship between land surface temperature and multiple vegetation indices. *Remote Sens Appl Soc Env* 7:57–68
- Amiri R, Weng Q, Alimohammadi A, Alavipanah SK (2009) Spatial-temporal dynamics of land surface temperature in relation to fractional vegetation cover and land use/cover in the Tabriz urban area, Iran. *Remote Sens Environ* 113(12):2606–2617. <https://doi.org/10.1016/j.rse.2009.07.021>
- Artis DA, Carnahan WH (1982) Survey of emissivity variability in thermography of urban areas. *Remote Sens Environ* 12(4):313–329. [https://doi.org/10.1016/0034-4257\(82\)90043-8](https://doi.org/10.1016/0034-4257(82)90043-8)
- Askne J, Santoro M, Smith G, Fransson JES (2003) Multitemporal repeat-pass SAR interferometry of boreal forests. *IEEE Trans Geosci Remote Sens* 41:1540–1550. <https://doi.org/10.1109/TGRS.2003.813397>
- Avdan U, Jovanovska G (2016) Algorithm for automated mapping of land surface temperature using LANDSAT 8 satellite data. *J Sens*. <https://doi.org/10.1155/2016/1480307>
- Bhatta B (2009) Analysis of urban growth pattern using remote sensing and GIS: a case study of Kolkata, India. *Int J Remote Sens* 30(18):4733–4746. <https://doi.org/10.1080/01431160802651967>
- Bhatti SS, Tripathi NK (2014) Built-up area extraction using Landsat 8 OLI imagery. *GIScience Remote Sens* 51(4):445–467. <https://doi.org/10.1080/15481603.2014.939539>
- Census of India (2011) Census of India 2011. Government of India http://censusindia.gov.in/DigitalLibrary/Archive_home.aspx
- Chen XL, Zhao HM, Li PX, Yin ZY (2006) Remote sensing image-based analysis of the relationship between urban heat island and land use/cover changes. *Remote Sens Environ* 104(2):133–146. <https://doi.org/10.1016/j.rse.2005.11.016>
- Chen J, Chang K, Karacsonyi D, Zhang X (2014) Comparing urban land expansion and its driving factors in Shenzhen and Dongguan, China. *Habitat Int* 43:61–71. <https://doi.org/10.1016/j.habitatint.2014.01.004>
- Congalton RG, Green K (2009) Assessing the accuracy of remotely sensed data: principles and practices. *Photogramm Rec*. https://doi.org/10.1111/j.1477-9730.2010.00574_2.x
- Connors JP, Galletti CS, Chow WTL (2013) Landscape configuration and urban heat island effects: assessing the relationship between landscape characteristics and land surface temperature in Phoenix, Arizona. *Landscape Ecol* 28(2):271–283. <https://doi.org/10.1007/s10980-012-9833-1>
- Crawley MJ (2007) *The R book*. Wiley, Hoboken. <https://doi.org/10.1002/9780470515075>
- Dasgupta S, Gosain AK, Rao S, Roy S, Sarraf M (2013) A megacity in a changing climate: the case of Kolkata. *Clim Change* 116(3–4):747–766. <https://doi.org/10.1007/s10584-012-0516-3>
- Decker EH, Elliott S, Smith FA, Blake DR, Rowland FS (2000) Energy and material flow through the urban ecosystem. *Annu Rev Energy Environ* 25:685–740. <https://doi.org/10.1146/annurev.energy.25.1.685>
- Deng C, Wu C (2013) A spatially adaptive spectral mixture analysis for mapping subpixel urban impervious surface distribution. *Remote Sens Environ* 133:62–70. <https://doi.org/10.1016/j.rse.2013.02.005>
- Dietz T, Rosa EA, York R (2007) Driving the human ecological footprint. *Front Ecol Environ* 5(1):13–18. [https://doi.org/10.1890/1540-9295\(2007\)5%5B13:DTHEF%5D2.0.CO;2](https://doi.org/10.1890/1540-9295(2007)5%5B13:DTHEF%5D2.0.CO;2)
- Drăguț L, Blaschke T (2006) Automated classification of landform elements using object-based image analysis. *Geomorphology* 81(3–4):330–344. <https://doi.org/10.1016/j.geomorph.2006.04.013>
- Erbek FS, Özkan C, Taberner M (2004) Comparison of maximum likelihood classification method with supervised artificial neural network algorithms for land use activities. *Int J Remote Sens* 25(9):1733–1748. <https://doi.org/10.1080/0143116031000150077>
- ERDAS (2009) *ERDAS field guide*™—tutorial. Imagine, Atlanta, Georgia
- Estoque RC, Murayama Y (2017) Monitoring surface urban heat island formation in a tropical mountain city using Landsat data (1987–2015). *ISPRS J Photogramm Remote Sens* 133:18–29
- Foody GM (1992) On the compensation for chance agreement in image classification accuracy assessment. *Photogramm Eng Remote Sens* 58(10):1459–1460
- Gábor P, Jombach S (2010) The relation between the biological activity and the land surface temperature in Budapest. *Appl Ecol Environ Res* 7(3):241–251
- Getis A, Ord JK (1992) The Analysis of spatial association by use of distance statistics. *Geogr Anal* 24(3):189–206. <https://doi.org/10.1111/j.1538-4632.1992.tb00261.x>
- Ghosh S, Dinda S, Chatterjee ND, Das K (2018) Analyzing risk factors for shrinkage and transformation of East Kolkata Wetland, India. *Spat Inf Res*. <https://doi.org/10.1007/s41324-018-0212-0>
- Grimm NB, Faeth SH, Golubiewski NE, Redman CL, Wu J, Bai X, Briggs JM (2008) Global change and the ecology of cities. *Science*. <https://doi.org/10.1126/science.1150195>
- Guo G, Wu Z, Xiao R, Chen Y, Liu X, Zhang X (2015) Impacts of urban biophysical composition on land surface temperature in urban heat island clusters. *Landscape Urban Plan* 135:1–10. <https://doi.org/10.1016/j.landurbplan.2014.11.007>
- Guo G, Zhou X, Wu Z, Xiao R, Chen Y (2016) Characterizing the impact of urban morphology heterogeneity on land surface temperature in Guangzhou, China. *Env Model Softw* 84:427–439. <https://doi.org/10.1016/j.envsoft.2016.06.021>
- Haas J, Ban Y (2014) Urban growth and environmental impacts in Jing-Jin-Ji, the Yangtze, River Delta and the Pearl River Delta. *Int J Appl Earth Obs Geoinf* 30(1):42–55. <https://doi.org/10.1016/j.jag.2013.12.012>
- Hoffmann P, Krueger O, Schlünzen KH (2012) A statistical model for the urban heat island and its application to a climate change scenario. *Int J Climatol* 32(8):1238–1248. <https://doi.org/10.1002/joc.2348>
- Huete AR (1988) A soil-adjusted vegetation index (SAVI). *Remote Sens Environ* 25(3):295–309. [https://doi.org/10.1016/0034-4257\(88\)90106-X](https://doi.org/10.1016/0034-4257(88)90106-X)
- Hull V, Tuanmu MN, Liu J (2015) Synthesis of human-nature feedbacks. *Ecol Soc* 20:3. <https://doi.org/10.5751/ES-07404-200317>
- Jiang J, Tian G (2010) Analysis of the impact of land use/land cover change on land surface temperature with remote sensing. *Procedia Environ Sci* 2:571–575. <https://doi.org/10.1016/j.proenv.2010.10.062>
- Jiménez-Muñoz JC, Sobrino JA, Gillespie A, Sabol D, Gustafson WT (2006) Improved land surface emissivities over agricultural areas using ASTER NDVI. *Remote Sens Environ* 103(4):474–487. <https://doi.org/10.1016/j.rse.2006.04.012>
- Jong R, de Bruin S, de Wit A, Schaepman ME, Dent DL (2011) Analysis of monotonic greening and browning trends from global NDVI time-series. *Remote Sens Environ* 115(2):692–702. <https://doi.org/10.1016/j.rse.2010.10.011>
- Julien Y, Sobrino JA (2009) The yearly land cover dynamics (YLCD) method: an analysis of global vegetation from NDVI and LST parameters. *Remote Sens Environ* 113(2):329–334. <https://doi.org/10.1016/j.rse.2008.09.016>

- Kalnay E, Cai M (2003) Impact of urbanization and land-use change on climate. *Nature* 423(May):528–532. <https://doi.org/10.1038/nature01649.1>
- Kates RW, Clark WC, Corell R, Hall JM, Jaeger CC, Lowe I, Svedin U (2001) Environment and development: sustainability science. *Science* 292(5517):641–642. <https://doi.org/10.1126/science.1059386>
- Khan A, Chatterjee S, Akbari H, Bhatti SS, Dinda A, Mitra C, Doan Q Van (2017) Step-wise land-class elimination approach for extracting mixed-type built-up areas of Kolkata megacity. *Geocarto Int*. <https://doi.org/10.1080/10106049.2017.1408704>
- KMDA (Kolkata Metropolitan Development Authority) (2011) KMDA annual report. http://www.kmdaonline.org/home/aar_2011. Accessed 27 Jul 2018
- Kuang W (2012) Spatio-temporal patterns of intra-urban land use change in Beijing, China between 1984 and 2008. *Chin Geogr Sci* 22(2):210–220. <https://doi.org/10.1007/s11769-012-0529-x>
- Li Y, Liu G (2017) Characterizing spatiotemporal pattern of land use change and its driving force based on GIS and landscape analysis techniques in Tianjin during 2000–2015. *Sustain (Switz)* 9:6. <https://doi.org/10.3390/su9060894>
- Li S, Ma Y (2014) Urbanization, economic development and environmental change. *Sustainability* 6(8):5143–5161. <https://doi.org/10.3390/su6085143>
- Li J, Wang X, Wang X, Ma W, Zhang H (2009) Remote sensing evaluation of urban heat island and its spatial pattern of the Shanghai metropolitan area, China. *Ecol Complex* 6(4):413–420. <https://doi.org/10.1016/j.ecocom.2009.02.002>
- Li B, Chen D, Wu S, Zhou S, Wang T, Chen H (2016a) Spatio-temporal assessment of urbanization impacts on ecosystem services: case study of Nanjing City, China. *Ecol Ind* 71:416–427. <https://doi.org/10.1016/j.ecolind.2016.07.017>
- Li L, Lu D, Kuang W (2016b) Examining urban impervious surface distribution and its dynamic change in Hangzhou metropolis. *Remote Sens* 8:3. <https://doi.org/10.3390/rs8030265>
- Liu F, Zhang Z, Shi L, Zhao X, Xu J, Yi L, Li M (2016) Urban expansion in China and its spatial-temporal differences over the past four decades. *J Geog Sci* 26(10):1477–1496. <https://doi.org/10.1007/s11442-016-1339-3>
- Liu Y, Song W, Deng X (2018) Understanding the spatiotemporal variation of urban land expansion in oasis cities by integrating remote sensing and multi-dimensional DPSIR-based indicators. *Ecol Ind*. <https://doi.org/10.1016/j.ecolind.2018.01.029>
- Lu X, Shi Y, Chen C, Yu M (2017) Monitoring cropland transition and its impact on ecosystem services value in developed regions of China: a case study of Jiangsu Province. *Land Use Policy* 69:25–40. <https://doi.org/10.1016/j.landusepol.2017.08.035>
- Maki M, Ishihara M, Tamura M (2004) Estimation of leaf water status to monitor the risk of forest fires by using remotely sensed data. *Remote Sens Environ* 90(4):441–450. <https://doi.org/10.1016/j.rse.2004.02.002>
- Markham BL, Barker JL (1985) Spectral characterization of the LANDSAT Thematic Mapper sensors. *Int J Remote Sens* 6(5):697–716. <https://doi.org/10.1080/01431168508948492>
- Mather PM (2004) Computer processing of remotely sensed images: an introduction, vol 4. Wiley, Chichester, pp 4–344. ISBN:9781280287527
- Mathew A, Khandelwal S, Kaul N (2017) Investigating spatial and seasonal variations of urban heat island effect over Jaipur city and its relationship with vegetation, urbanization and elevation parameters. *Sustain Cities Soc* 35:157–177. <https://doi.org/10.1016/j.scs.2017.07.013>
- Maxwell SK, Sylvester KM (2012) Identification of “ever-cropped” land (1984–2010) using Landsat annual maximum NDVI image composites: Southwestern Kansas case study. *Remote Sens Environ* 121:186–195. <https://doi.org/10.1016/j.rse.2012.01.022>
- McFeeters SK (1996) The use of the normalized difference water index (NDWI) in the delineation of open water features. *Int J Remote Sens* 17(7):1425–1432. <https://doi.org/10.1080/01431169608948714>
- Mithun S, Chattopadhyay S, Bhatta B (2016) Analyzing urban dynamics of metropolitan Kolkata, India by using landscape metrics. *Papers Appl Geogr* 2(3):284–294. <https://doi.org/10.1080/23754931.2016.1148069>
- Mitra P, Shankar BU, Pal SK (2004) Segmentation of multispectral remote sensing images using active support vector machines. *Pattern Recogn Lett* 25(9):1067–1074
- Monserud RA, Leemans R (1992) Comparing global vegetation maps with the Kappa statistic. *Ecol Model* 62(4):275–293. [https://doi.org/10.1016/0304-3800\(92\)90003-W](https://doi.org/10.1016/0304-3800(92)90003-W)
- Mukherjee J (2015) Beyond the urban: rethinking urban ecology using Kolkata as a case study. *Int J Urban Sustain Dev* 7(2):131–146. <https://doi.org/10.1080/19463138.2015.1011160>
- Mushore TD, Mutanga O, Odindi J, Dube T (2017) Assessing the potential of integrated Landsat 8 thermal bands, with the traditional reflective bands and derived vegetation indices in classifying urban landscapes. *Geocarto Int* 32(8):886–899. <https://doi.org/10.1080/10106049.2016.1188168>
- Ng CN, Xie YJ, Yu XJ (2011) Measuring the spatio-temporal variation of habitat isolation due to rapid urbanization: a case study of the Shenzhen River cross-boundary catchment, China. *Landsc Urban Plan* 103(1):44–54. <https://doi.org/10.1016/j.landurbplan.2011.05.011>
- Nichol JE (1994) A GIS-based approach to microclimate monitoring in Singapore’s high-rise housing estates. *Photogramm Eng Remote Sens* 60(10):1225–1232
- Oke TR (1987) Boundary layer climates. 2nd ed. London and New York: Routledge. *J Chem Inf Model*. <https://doi.org/10.1017/CBO9781107415324.004>
- Otukei JR, Blaschke T (2010) Land cover change assessment using decision trees, support vector machines and maximum likelihood classification algorithms. *Int J Appl Earth Obs Geoinf* 12(SUPPL. 1):S27–S31. <https://doi.org/10.1016/j.jag.2009.11.002>
- Owen TW, Carlson TN, Gillies RR (1998) An assessment of satellite remotely-sensed land cover parameters in quantitatively describing the climatic effect of urbanization. *Int J Remote Sens* 19(9):1663–1681. <https://doi.org/10.1080/014311698215171>
- Pal S, Ziaul S (2017) Detection of land use and land cover change and land surface temperature in English Bazar urban centre. *Egypt J Remote Sens Space Sci* 20(1):125–145. <https://doi.org/10.1016/j.ejrs.2016.11.003>
- Popa P, Timofti M, Voiculescu M, Dragan S, Trif C, Georgescu LP (2012) Study of physico-chemical characteristics of wastewater in an urban agglomeration in Romania. *Sci World J*. [doi:https://doi.org/10.1100/2012/549028](https://doi.org/10.1100/2012/549028)
- Punia M, Singh L (2012) Entropy approach for assessment of urban growth: a case study of Jaipur, India. *J Indian Soc Remote Sens* 40(2):231–244. <https://doi.org/10.1007/s12524-011-0141-z>
- Qin Z, Karnieli A, Berliner P (2001) A mono-window algorithm for retrieving land surface temperature from Landsat TM. *Int J Remote Sens* 22(18):3719–3746. <https://doi.org/10.1080/01431160010006971>
- Rahman A, Aggarwal SP, Netzband M, Fazal S (2011) Monitoring urban sprawl using remote sensing and GIS techniques of a fast growing urban centre, India. *IEEE J Select Top Appl Earth Obs Remote Sens* 4(1):56–64. <https://doi.org/10.1109/jstars.2010.2084072>

- Ramachandra TV, Aithal BH, Sowmyashree MV (2014) Urban structure in Kolkata: metrics and modelling through geo-informatics. *Appl Geomat* 6(4):229–244. <https://doi.org/10.1007/s12518-014-0135-y>
- Ranagalage M, Estoque RC, Zhang X, Murayama Y (2018a) Spatial changes of urban heat island formation in the Colombo District, Sri Lanka: implications for sustainability planning. *Sustain* (Switz). <https://doi.org/10.3390/su10051367>
- Ranagalage M, Dissanayake DMSLB, Murayama Y, Zhang X, Estoque R, Perera ENC, Morimoto T (2018b) Quantifying surface urban heat island formation in the world heritage tropical mountain city of Sri Lanka. *ISPRS Int J Geo Inf* 7(9):341
- Ranagalage M, Estoque R, Handayani H, Zhang X, Morimoto T, Tadono T, Murayama Y (2018c) Relation between urban volume and land surface temperature: a comparative study of planned and traditional cities in Japan. *Sustainability*. 10(7):2366. <https://doi.org/10.3390/su10072366>
- Raynolds MK, Comiso JC, Walker DA, Verbyla D (2008) Relationship between satellite-derived land surface temperatures, arctic vegetation types, and NDVI. *Remote Sens Environ* 112(4):1884–1894. <https://doi.org/10.1016/j.rse.2007.09.008>
- Ren W, Zhong Y, Meligrana J, Anderson B, Watt WE, Chen J, Leung HL (2003) Urbanization, land use, and water quality in Shanghai 1947–1996. *Environ Int* 29(5):649–659. [https://doi.org/10.1016/S0160-4120\(03\)00051-5](https://doi.org/10.1016/S0160-4120(03)00051-5)
- Sahana M, Hong H, Sajjad H (2018) Analyzing urban spatial patterns and trend of urban growth using urban sprawl matrix: a study on Kolkata urban agglomeration, India. *Sci Total Environ* 628–629:1557–1566. <https://doi.org/10.1016/j.scitotenv.2018.02.170>
- Sandholt I, Rasmussen K, Andersen J (2002) A simple interpretation of the surface temperature/vegetation index space for assessment of surface moisture status. *Remote Sens Environ* 79(2–3):213–224. [https://doi.org/10.1016/S0034-257\(01\)00274-7](https://doi.org/10.1016/S0034-257(01)00274-7)
- Sannigrahi S, Bhatt S, Rahmat S, Uniyal B, Banerjee S, Chakraborti S, Bhatt A (2017) Analyzing the role of biophysical compositions in minimizing urban land surface temperature and urban heating. *Urban Clim*. <https://doi.org/10.1016/j.uclim.2017.10.002>
- Santos dos AR, de Oliveira FS, da Silva AG, Gleriani JM, Gonçalves W, Moreira GL, Mota PHS (2017) Spatial and temporal distribution of urban heat islands. *Sci Total Environ* 605–606:946–956
- Scolozzi R, Geneletti D (2012) A multi-scale qualitative approach to assess the impact of urbanization on natural habitats and their connectivity. *Env Impact Assess Rev* 36:9–22. <https://doi.org/10.1016/j.eiar.2012.03.001>
- Sharma R, Ghosh A, Joshi PK (2013) Analysingspatio-temporal footprints of urbanization on environment of Surat city using satellite-derived bio-physical parameters. *Geocarto Int* 28(5):420–438. <https://doi.org/10.1080/10106049.2012.715208>
- Sharma R, Chakraborty A, Joshi PK (2015) Geospatial quantification and analysis of environmental changes in urbanizing city of Kolkata (India). *Environ Monit Assess* 187(1):4206. <https://doi.org/10.1007/s10661-014-4206-7>
- Shi Y, Katschnner L, Ng E (2018) Modelling the fine-scale spatiotemporal pattern of urban heat island effect using land use regression approach in a megacity. *Sci Total Environ* 618:891–904. <https://doi.org/10.1016/j.scitotenv.2017.08.252>
- Shifaw E, Sha J, Li X, Bao Z, Ji J, Chen B (2018) Spatiotemporal analysis of vegetation cover (1984–2017) and modelling of its change drivers, the case of Pingtan Island, China. *Model Earth Syst Env*. <https://doi.org/10.1007/s40808-018-0473-6>
- Shiflett SA, Liang LL, Crum SM, Feyisa GL, Wang J, Jenerette GD (2017) Variation in the urban vegetation, surface temperature, air temperature nexus. *Sci Total Environ* 579:495–505. <https://doi.org/10.1016/j.scitotenv.2016.11.069>
- Sobrino JA, Jiménez-Muñoz JC, Paolini L (2004) Land surface temperature retrieval from LANDSAT TM 5. *Remote Sens Environ* 90(4):434–440. <https://doi.org/10.1016/j.rse.2004.02.003>
- Sudhira HS, Ramachandra TV, Jagadish KS (2004) Urban sprawl: metrics, dynamics and modelling using GIS. *Int J Appl Earth Obs Geoinf* 5(1):29–39. <https://doi.org/10.1016/j.jag.2003.08.002>
- Sun Y, Zhao S (2018) Spatiotemporal dynamics of urban expansion in 13 cities across the Jing-Jin-Ji urban agglomeration from 1978 to 2015. *Ecol Ind* 87:302–313. <https://doi.org/10.1016/j.ecoli.2017.12.038>
- Sun Y, Zhao S, Qu W (2015) Quantifying spatiotemporal patterns of urban expansion in three capital cities in Northeast China over the past three decades using satellite data sets. *Env Earth Sci* 73(11):7221–7235. <https://doi.org/10.1007/s12665-014-3901-6>
- Sun Z, Wu F, Shi C, Zhan J (2016) The impact of land use change on water balance in Zhangye city, China. *Phys Chem Earth* 96:64–73. <https://doi.org/10.1016/j.pce.2016.06.004>
- Townshend JRG, Justice CO (1986) Analysis of the dynamics of African vegetation using the normalized difference vegetation index. *Int J Remote Sens* 7(11):1435–1445. <https://doi.org/10.1080/01431168608948946>
- Tran DX, Pla F, Latorre-Carmona P, Myint SW, Caetano M, Kieu HV (2017) Characterizing the relationship between land use land cover change and land surface temperature. *ISPRS J Photogramm Remote Sens* 124:119–132. <https://doi.org/10.1016/j.isprsjprs.2017.01.001>
- Trlica A, Hutyrá LR, Schaaf CL, Erb A, Wang JA (2017) Albedo, land cover, and daytime surface temperature variation across an urbanized landscape. *Earth's Futur* 5(11):1084–1101. <https://doi.org/10.1002/2017EF000569>
- United Nations (2014) World urbanization prospects. World urbanization prospects: the 2014 revision highlights. <https://doi.org/10.4054/DemRes.2005.12.9>
- USGS (2015) Landsat 8 (L8) Data Users Handbook. Earth Resources Observation and Science (EROS) Center, vol 8. <http://landsat.usgs.gov/documents/Landsat8DataUsersHandbook.pdf>. Accessed 5 Mar 2018
- USGS (2016) Landsat 8 (L8) Data Users Handbook. Department of the Interior US Geological Survey. http://landsat.usgs.gov/sites/default/files/documents/LSDS-1574_L8_Data_Users_Handbook.pdf. Accessed 12 Apr 2018
- Van der Linden S, Janz A, Waske B, Eiden M, Hostert P (2007) Classifying segmented hyperspectral data from a heterogeneous urban environment using support vector machines. *J Appl Remote Sens* 1(1):13543. doi:<https://doi.org/10.1117/1.2813466>
- Voogt JA, Oke TR (2003) Thermal remote sensing of urban climates. *Remote Sens Environ* 86(3):370–384. [https://doi.org/10.1016/S0034-4257\(03\)00079-8](https://doi.org/10.1016/S0034-4257(03)00079-8)
- Wang YC, Hu BKH, Myint SW, Feng CC, Chow WTL, Passy PF (2018) Patterns of land change and their potential impacts on land surface temperature change in Yangon, Myanmar. *Sci Total Environ*. <https://doi.org/10.1016/j.scitotenv.2018.06.209>
- Weng Q, Lu D, Schubring J (2004) Estimation of land surface temperature-vegetation abundance relationship for urban heat island studies. *Remote Sens Environ* 89(4):467–483. <https://doi.org/10.1016/j.rse.2003.11.005>
- Weng QH, Lu DS, Liang BQ (2006) Urban surface biophysical descriptors and land surface temperature variations. *Photogramm Eng Remote Sens* 72(11):1275–1286. <https://doi.org/10.14358/PERS.72.11.1275>
- Weng Q, Liu H, Liang B, Lu D (2008) The spatial variations of urban land surface temperatures: pertinent factors, zoning effect, and seasonal variability. *IEEE J Sel Top Appl Earth Obs Remote Sens* 1:2. <https://doi.org/10.1109/JSTARS.2008.917869>

- Wulder M, Boots B (1998) Local spatial autocorrelation characteristics of remotely sensed imagery assessed with the Getis statistic. *Int J Remote Sens* 19(11):2223–2231. <https://doi.org/10.1080/01431698214983>
- Xiao H, Weng Q (2007) The impact of land use and land cover changes on land surface temperature in a karst area of China. *J Env Manage* 85(1):245–257. <https://doi.org/10.1016/j.jenvman.2006.07.016>
- Xu H (2006) Modification of normalised difference water index (NDWI) to enhance open water features in remotely sensed imagery. *Int J Remote Sens* 27(14):3025–3033. <https://doi.org/10.1080/01431160600589179>
- Xu HQ, Chen BQ (2004) Remote sensing of the urban heat island and its changes in Xiamen City of SE China. *J Environ Sci (China)* 16(2):276–281
- Yang L, Liu N, Dai MZ, Lu GF (2008) Calculation and analysis on the eco-environmental pressure from residents' living consumption in the progress of rapid urbanization: a case study on Jiangyin City, Jiangsu Province, Shengtai Xuebao. *Acta Ecol Sin* 28:5610–5618
- Yeh AG, Li X (2001) Measurement and monitoring of urban sprawl in a rapidly growing region using entropy. *Photogramm Eng Remote Sens* 67(1):83–90
- Yue W, Xu J, Tan W, Xu L (2007) The relationship between land surface temperature and NDVI with remote sensing: application to Shanghai Landsat 7 ETM + data. *Int J Remote Sens* 28(15):3205–3226. <https://doi.org/10.1080/01431160500306906>
- Zha Y, Gao J, Ni S (2003) Use of normalized difference built-up index in automatically mapping urban areas from TM imagery. *Int J Remote Sens* 24(3):583–594. <https://doi.org/10.1080/01431160304987>
- Zhang Y, Odeh IOA, Han C (2009) Bi-temporal characterization of land surface temperature in relation to impervious surface area, NDVI and NDBI, using a sub-pixel image analysis. *Int J Appl Earth Obs Geoinf* 11(4):256–264. <https://doi.org/10.1016/j.jag.2009.03.001>
- Zhang M, Zhou Y, Liu X, Lu Z (2017) Ecological landscape regulation approaches in Xilingol, Inner Mongolia: an urban ecosystem services perspective. *Int J Sustain Dev World Ecol* 24(5):401–407. <https://doi.org/10.1080/13504509.2016.1273263>
- Zhou Q, Robson M, Pilesjo P (1998) On the ground estimation of vegetation cover in Australian rangelands. *Int J Remote Sens* 19(9):1815–1820. <https://doi.org/10.1080/014311698215261>
- Zhou L, Dickinson RE, Tian Y, Fang J, Li Q, Kaufmann RK, Myneni RB (2004) Evidence for a significant urbanization effect on climate in China. *Proc Natl Acad Sci* 101(26):9540–9544. <https://doi.org/10.1073/pnas.0400357101>
- Zhou W, Huang G, Cadenasso ML (2011) Does spatial configuration matter? Understanding the effects of land cover pattern on land surface temperature in urban landscapes. *Landsc Urban Plan* 102(1):54–63. <https://doi.org/10.1016/j.landurbplan.2011.03.009>
- Zhu W, Lü A, Jia S (2013) Estimation of daily maximum and minimum air temperature using MODIS land surface temperature products. *Remote Sens Env* 130:62–73. <https://doi.org/10.1016/j.rse.2012.10.034>